



The recovery and re-calibration of a 13-month aerosol extinction profiles dataset from searchlight observations from New Mexico, after the 1963 Agung eruption.

5 Juan-Carlos Antuña-Marrero¹, Graham W. Mann^{2,3}, John Barnes⁴, Abel Calle¹, Sandip S. Dhomse^{2,5}, Victoria E. Cachorro Revilla¹, Terry Deshler⁶, Li Zhengyao², Nimmi Sharma⁷ and Louis Elterman^{8†}

¹Group of Atmospheric Optics (GOA-UVa), Universidad de Valladolid, 47011, Valladolid, Spain

10 ²School of Earth and Environment, University of Leeds, Leeds, LS2 9JT, UK

³National Centre for Atmospheric Science (NCAS-Climate), University of Leeds, Leeds, LS2 9JT, UK

⁴NOAA ESRL Global Monitoring Laboratory, Boulder, CO, USA

⁵National Centre for Earth Observation (NCEO), University of Leeds, Leeds, LS2 9JT, UK

⁶Laboratory for Atmospheric and Space Physics, University of Colorado at Boulder, Boulder, Colorado, 80303, USA

15 ⁷Department of Physics and Earth Sciences, Central Connecticut State University, CT, USA

⁸Air Force Geophysics Laboratory (AFSC), Hanscom Air Force Base, MA, USA

20 Correspondence to: Juan-Carlos Antuña-Marrero (antuna@goa.uva.es)

Submitted to: Earth System Science Data Journal on August 20, 2022



25 **Abstract:** We report the recovery and re-calibration of an extensive dataset of vertical profile measurements of the
1963/64 stratospheric aerosol layer measured from a two-site searchlight measurement facility at White Sands missile
base and Sacramento Peak observatory, in New Mexico, US. The recovered dataset comprises 105 profiles of 550nm
aerosol extinction ($\beta_p(z)$) and is part of a longer program of measurements with the US Air Force Cambridge Research
Laboratories (AFCRL) searchlight facility that began in February 1963. The recovered series of $\beta_p(z)$ profiles span the
30 13-month period December 1963 to December 1964 and provide a unique record of the altitude and vertical extent of the
Northern Hemisphere dispersed portion of the aerosol cloud from the March 1963 Agung volcanic eruption. The data
recovery methodology involved first re-digitizing the 105 original $\beta_p(z)$ profiles ($\beta_p^{Orig}(z)$) from individual Figures
within an AFCRL research report (Elterman, 1966a). The re-calibration involves inverting the original equation used to
compute $\beta_p(z)$ in Elterman (1966a; 1966b) to retrieve a normalized detector response ($\frac{E_{rp}(z)}{E_{rp}(35)}$) profile for each of the 105
35 re-digitized $\beta_p^{Orig}(z)$ profiles. An iterative procedure was then used to compute the re-calibration $\beta_p^{Orig}(z)$ profiles
($\beta_p^{Recal}(z)$), with the molecular extinction profile calculated with the corresponding daily molecular extinction profile
calculated from local soundings, rather than the US Standard Atmosphere 1962 in the original dataset. Two-way
molecular and aerosol transmittance corrections are applied using the MODTRAN (MODerate resolution atmospheric
TRANsmission) code in transmission mode, applying a best-estimate aerosol phase function calculated from
40 measurements, applied for the entire 2.76 to 35.2 km column. For the tropospheric aerosol transmittance, the AERONET
aerosol phase function from White Sands High Energy Laser Systems Test Facility (HELSTF) was applied (2.76 to 10.7
km), a separate stratospheric phase function applied between 11.2 and 35.2 km, calculated from a set of particle size
distributions measured by the U-2 high-altitude aircraft over a US region in the vicinity of White Sands in early 1964.
Errors were estimated taking as a reference the errors determined in the computation of $\beta_p^{Orig}(z)$. Using available
45 tabulated data from the original procedure the errors in the re-digitalization of $\beta_p^{Orig}(z)$ and in the retrieval of the $\frac{E_{rp}(z)}{E_{rp}(35)}$
procedures were calculated and later added to the original estimates. Both the $\beta_p^{Recal}(z)$ and the stratospheric aerosol
optical depth magnitudes showed higher magnitudes than $\beta_p^{Orig}(z)$ and the original stratospheric aerosol optical depth,
however their magnitudes show a reasonable agreement with other contemporary observations. Both the original and re-
calibration datasets are being submitted to PANGAEA data repository for its storage and public access.

50



1 Introduction

Substantial advances in our understanding of large-magnitude explosive volcanic aerosol physico-chemical processes and radiative forcings (e.g. Timmreck, 2012), and the sometimes complex interactions with the earth's surface climate (e.g. Rocco, 2000) and atmospheric composition (Kremser et al., 2016). Current international scientific cooperation on this subject includes two series of multi-model experiments, each investigating a different aspect of the atmospheric effects from the largest volcanic eruptions of the last century. The VolMIP initiative (Zanchettin et al., 2016) is exploring the climate response to major volcanic eruptions (e.g., Zanchettin et al., 2022), aligned to the CMIP6 climate modelling activity. Additionally to VolMIP, the ISA-MIP initiative (Timmreck et al., 2018), focuses on the aerosol radiative forcing from major eruptions, organized within the frame of the Stratospheric Sulfur and its Role in Climate (SSiRC) initiative, itself part of the World Climate Research Program's SPARC initiative (Stratosphere-troposphere Processes And their Role in Climate). The HERSEA experiment within ISA-MIP focuses on the formation and global dispersion of the volcanic aerosol clouds from the three largest tropical eruptions of the 20th century: Agung, El Chichón, and Pinatubo (see e.g., Dhomse et al., 2020). Of these eruptions, the Agung aerosol cloud is particularly uncertain, a recent analysis re-assessing the variability in and global distribution of the Agung aerosol cloud (Niemeier et al., 2019), raising again the issue of the few available observational datasets, and highlighting the large change in the CMIP6 volcanic forcing datasets for the Agung period (Luo, 2016) compared to the main dataset used for CMIP5 (Sato et al., 1993).

Substantial uncertainty is also present for the 1982 El Chichón eruption (the forcing relying primarily on aircraft lidar measurements (e.g. McCormick and Swissler, 1983) and to some extent also for the 1991 Pinatubo eruption, to the SAGE-II gap period (Thomason et al., 2018). The potential for other measurement datasets to potentially reduce the uncertainty in these strong radiative forcings, is the primary motivation for a "Data Rescue activity" within SSiRC, specifically focused on the periods after major volcanic eruptions (<http://www.sparc-ssirc.org/data/datarescueactivity.html>).

The first phase of the SSiRC Data activity has recovered two important lidar aerosol extinction profile datasets, each adding new constraints for 1 of the major volcanic aerosol clouds in the ISA-MIP HERSEA activity. Firstly, for the uncertain tropical portion of the Pinatubo aerosol cloud, a series of ship-borne lidar aerosol extinction profiles from two series of trans-Atlantic cruises with different Soviet vessels in July to September 1991, and in January and February 1992 (see Antuña-Marrero et al., 2020). The Professor Zubov ship crossed the Atlantic from Europe to the Caribbean (~40° to 8° N) between July and September 1991 and Professor Vize from Europe to south of the Equator (~4° N to 8° S) between January and February 1992. Secondly, for the uncertain Agung aerosol forcing, the first ever multi-year program of ground-based lidar measurements were recovered and re-calibrated, made from Lexington, Massachusetts from January 1964 to August 1965 (Antuña-Marrero et al., 2021).

This article reports the recovery and re-calibration of an even earlier active remote sensing dataset of the Northern Hemisphere dispersed Agung aerosol cloud, 550nm aerosol extinction profiles from a searchlight at White Sands (~32° N), New Mexico, US, between December 1963 and December 1964, this being one part of the 7-year program of measurements made from the searchlight facility between February 1963 and November 1970 (Elterman et al., 1973).

1.1 A brief historical context for the searchlight atmospheric profiling technique:

Although a review of the searchlight technique for atmospheric scattering measurements might be considered beyond the scope of this article, we choose to provide, as part of the recovery methodology paper, also some historical context for preceding research that progressed to the 1963-1970 AFCRL program of measurements from New Mexico. The application of the searchlight apparatus for atmospheric research was first proposed by Synge (1930). Tuve et al., (1935) described and tested in a laboratory a method to reach high altitude levels by modulating a searchlight beam, using a resonant amplifier to select a modulating frequency allowing to discriminate the scattered light from that from the night sky. A phototube was required for detection. The work in this field continued and in 1937 the first experiment measuring



the light scattered from a beam in a region above the tropopause, up to 22 km, was reported (Hulburt, 1937). The detection
95 method was photographing the beam instead of the modulating method cited above. Measured brightness for various
altitudes up to 22 km were compared with theoretical brightness of the beam, showing evidence of non-Rayleigh
scattering below 11km. Two years later, using a beam modulated with a rotating shutter, scattering was measured up to
25 km showing good agreement between the measurements and the theory above 8 km, assuming non-Rayleigh scattering
as the primary reason for the discrepancies found below 8 km (Johnson et al., 1939).

100 The searchlight technique continued its development with newer instruments used for atmospheric density measurements
in several countries such as the US (Friedland et al., 1956), the United Kingdom (Dodd, 1959), the former Soviet Union
(Rozenberg, 1960). However, the invention of the laser by Maiman (1960), supported by theoretical work on the extension
of maser technology to the infrared and visible regions of the spectrum (Schawlow and Townes, 1958) led to the
replacement of searchlight projectors by lasers and the birth of lidar. Nevertheless, searchlight measurements of the
105 stratospheric aerosols continued at White Sands, New Mexico until May 1975 (Elterman, 1976).

1.2 The New Mexico searchlight observations and the SSiRC focus on the Agung aerosol cloud:

The searchlight dataset recovery is the third post-Agung dataset to be rescued and re-calibration within the SSiRC data
rescue activity, the first two datasets also part of the US AFCRL measurement program. Firstly, a 20-month program of
110 66 lidar profile measurements of 694nm attenuated backscatter from Lexington, MA, between January 1964 and August
1965 (Grams and Fiocco, 1967), were recovered from dataset Tables within a PhD thesis from Massachusetts Institute
for Technology (Grams, 1966). The recovered 694nm measurements re-calibration and converted to the main 550nm
mid-visible wavelength (Antuña Marrero et al., 2021), this chosen for maximum alignment to the HERSEA-Agung
experiment within the ISA-MIP activity for interactive stratospheric aerosol models (Timmreck et al., 2018). Secondly,
115 within the same ESSD paper, a high-latitude dataset from nine additional AFCRL lidar profiles from College, Alaska,
during July and August 1964, recovered also from Gerald Grams's PhD thesis, were also re-calibrated, the two datasets
both published within an open access data repository (Antuña Marrero et al., 2020b). The re-calibration methodology in
both datasets principally involved applying two-way transmittance corrections for atmospheric molecular density,
tropospheric and stratospheric aerosols and ozone profiles (see Antuña-Marrero et al., 2021).

120 Together with the 1964/65 rescued and re-calibration aerosol extinction profiles from Lexington, MA and Fairbanks, AK,
the White Sands, NM dataset presented in this work will provide a 21-month dataset for the vertical profile evolution of
the NH-dispersed portion of the Agung aerosol cloud, complimenting gaps in the Lexington record, for a complete record
from December 1963 through to August 1965.

The rescued and re-calibration dataset of stratospheric aerosols extinction profiles reported in this article are derived from
125 searchlight measurements conducted at White Sands, New Mexico, US, between December 1963 and December 1964.
The earlier available report of the searchlight measurements in New Mexico reported measurements between August and
November 1950 near Albuquerque, New Mexico (Elterman, 1951). They used a searchlight projector that was installed
at Cedro Peak (2.36 km a.s.l.) and the detector at Sandia Crest (3.54 km a.s.l.), with a distance of 20.5 km between both,
still reporting measurements at this site in 1952 Elterman et al., (1954). Later, Elterman and Campbell (1964) described
130 the installation of the searchlight at White Sands (1.39 km a.s.l.) and the detector at Sacramento Peak (2.76 km a.s.l.),
with a distance of 30 km between both instruments. They also reported the observation conducted on 15 March 1964 at
02:35 MST (Figures 2 and 3). Further, the same scene geometry as in Elterman and Campbell (1964) is reported in Figure
1 of Elterman (1966b), except that the distance between instruments is reported as 30.2 km.

Our approach involves first applying the original methodologies and measurements conducted more than 50 years ago,
135 and aligns with the philosophy of the SSiRC data rescue activity to secure and preserve the detailed information included



in the reports (where possible), and we aim to apply and explain the original nomenclature and variable symbols used in the parent articles and reports.

It should be noted that, whereas today the terms extinction and attenuation are used inter-changeably, and represent the same physical quantity, within the AFCRL report (Elterman, 1966a), the term “extinction” was used only for the sum of aerosol and Rayleigh extinctions, the term “attenuation” used when referring to the component Rayleigh/molecular and aerosol extinctions. This distinction is illustrated on page 11, 2nd paragraph, 2nd sentence in Elterman, (1966a) and in Elterman (1964b) page 13, section 5.1, definition of Eq. (8). Within this article however, we use the term extinction in all cases (rather than attenuation), the precursor words “molecular/Rayleigh”, “aerosol” or “total” then specifying the corresponding quantity.

In section 2 the searchlight instrument is described, and the equation used for computing the aerosol extinction profiles is explained. Section 3 describes the methods used to re-digitize the aerosol extinction profiles from the AFCRL report figures and to evaluate the error in this initial step of the dataset’s recovery. Section 4 explains the procedure for retrieving the normalized detector response, the variables used, and an evaluation of the errors in that main component of the re-calibration. This section includes the description of the parameters used to compute the re-calibration aerosol extinction profiles. Section 5 presents the re-calibration aerosol extinction and a timeseries of the stratospheric optical depth, comparing also to the original AFCRL report dataset and two observation based Agung datasets (Sato et al., 1993; Stothers, 2001). Those results are discussed and also the estimated errors in the whole procedure from the re-digitized to the re-calibration aerosol extinction are explained.

2 Searchlight instrument and observations processing

Searchlight measurements of stratospheric density were reported by Elterman (1951) between August and November 1950 near Albuquerque, New Mexico. The searchlight projector was installed at Cedro Peak (2.36 km a.s.l.) and the detector at Sandia Crest (3.54 km a.s.l.), with a distance of 20.5 km between both. Elterman et al., (1954) still reports measurements at this site in 1952.

In 1964 a new searchlight setup for aerosol measurements both in the troposphere and in the stratosphere was reported operative with the detector at Sacramento Peak (32°47'N, 105°49'W, 2.76 km a.s.l.) at 30 km from the projector, whose exact location was not identified (Elterman and Campbell 1964a). The projector location was later reported to be at Two Buttes (also called Twin Buttes) 32°42'N, 106°08'W, 1388m (Hinds et al, 1975).

The searchlight geometry is shown in Fig. 1 from Elterman and Campbell (1964) and reproduced here as Fig.1 also. The instrument consisted in a beam from a searchlight (the projector) collimated by a 36-inch mirror and modulated by shutters at 33 cycles sec⁻¹. Synchronous demodulation enabled the use of very narrow frequency bandwidth for those times. The source intensity was measured by an auxiliary detector, mounted on the searchlight and also generated a signal synchronous with the modulation. The intensity level and synchronous signal were transmitted by conventional telephone to a site around 30 km distant, where the optical collector, synchronous rectifier-amplifier and recorder were located. The beam elevation angle was fixed, while the collector mirror scanned up and down the beam, providing a continuous record of scattered light intensity as a function of altitude. For the detection a photomultiplier was used with a 550 nm filter with a FWHM of 55 nm. The monitored source intensity, the scattered light intensity and the elevation angle of the collecting mirror were recorded simultaneously on a chart paper. The 30-km baseline was chosen to provide good spatial resolution for the measurements. The starting altitude of the upward scan (0° elevation of the collector mirror) was 2.76 km above sea level.



2.2 Searchlight observations and its original processing:

180 The rescued dataset consists of 105 aerosol extinction profiles for altitudes between 2.76 and 35 km, measured during the period 12 December 1963 through 12 December 1964 (Elterman, 1966a). Individual searchlight aerosol extinction observations were conducted between sunset and sunrise. The date of each consecutive set of observations from sunset to sunrise was selected from the date at 00:00 MST resulting in 36 nights of observations with the number of observations ranging from 1 to a maximum of 7 per night and average of 3 per night. Table T1 (Supplement) lists the observations grouped by the nights they were conducted.

185 According to Elterman (1966a) five main factors limited the number of profiles acquired in the cited period. They were (textually):

(1) The operational time that could be allowed was limited.

(2) Operations were conducted only during moonless nights in order to keep noise background at a minimum.

190 (3) Operations were canceled when meteorological conditions were unfavorable. This included high winds as well as cloudy skies. July and August seasonally are months when both dust storms and cloudy skies occur daily in New Mexico.

(4) Equipment difficulties accounted for absence of data in January 1964 and at other times.

(5) Failure of site facilities, especially telephone lines, resulted in considerable loss of time. Synchronous rectification and amplification depended on transmission of the synchronizing signal by telephone.

195 The processing of the searchlight observations we rescued used the so-called linear iterative method to derive the vertical profiles of aerosol extinction. The linear iterative method, introduced by Elterman (1966 a, b), together with the Fernald (1972) and Klett (1985) methods are among the most commonly used to derive aerosol extinction and scatter coefficients from lidar signals (Kovalev, 2004).

200 Applying the energy transfer equations to the scene geometry shown in figure 1, assuming the aerosol extinction around 35 km is sufficiently small to be neglected and normalizing to unity at 35.3 km, the aerosol extinction coefficient ($\beta_p(h)$ in km^{-1}) was derived (Elterman 1966a, b):

$$\beta_p(z) = \frac{E_{rp}(z)}{E_{rp}(35)} \frac{T_r(35)}{T_r(z)} \frac{T_p(35)}{T_p(z)} \beta_R(35) \frac{P_R(132^\circ)}{P_p(\varphi_s(z))} - \beta_R(z) \frac{P_R(\varphi_s(z))}{P_p(\varphi_s(z))} \quad (1)$$

where z is the altitude (km), $E_{rp}(z)$ is the instrumentation response (volts), $\frac{E_{rp}(z)}{E_{rp}(35)}$ is the normalized detector response

205 with respect to $E_{rp}(35)$, $\beta_p(z)$ the aerosol extinction coefficient (km^{-1}), $\beta_R(z)$ the molecular extinction coefficient (km^{-1}), $P_p(\varphi_s(z))$ the normalized aerosol phase function (sr^{-1}), $P_R(\varphi_s(z))$ the normalized molecular phase function (sr^{-1}), $\varphi_s(z)$ scattering angle, $T_p(z)$ and $T_r(z)$ aerosol and molecular transmission respectively for both slant paths.

Vertical profiles of $T_p(z)^{Init}$ and $T_r(z)$ were derived using vertical profiles of $\beta_p(z)$ and $\beta_R(z)$ from the Atmospheric Attenuation Model (Elterman, 1964b), using the equation. (15) reported by Elterman (1966b). Since $T_p(z)$ is a function of $\beta_p(z)$, after the initial $\beta_p(z)$ is calculated using $T_p(z)^{Init}$, an iterative convergent method was then applied (Elterman

210 1966a, b).

The solution of equation (1) is not analytic, because $T_p(z)$ is a function of $\beta_p(z)$. Therefore an iterative-convergent procedure was applied. The iterative method began by first calculating an initial profile of $T_p(z)$, that we denote as $T_p(z)^{Orig}$ using the $\beta_p(z)^{Orig}$ at 550 nm from the Atmospheric Attenuation Model (Elterman, 1964b). Then $T_p(z)^{Orig}$ was used to derive the initial profiles of $\beta_p(z)$ and the iteration procedure of $T_p(z)$ and $\beta_p(z)$ calculus began until convergence was reached. Then the final set of $\beta_p(z)$ profiles (the solutions of the iterative method) constitutes the dataset reported in Elterman (1966a), i.e. the symbols shown in the AFCRL report Figures, which we re-digitized.

Two main issues limit this work to a re-calibration of the rescued dataset instead of a full recalculation including the iterative-convergent procedure for $T_p(z)$ and $\beta_p(z)$. The first originates in the normalization of the detector response



applied in deriving equation (1). In some cases the measured profile lacked data about $E_{rp}(35)$ and in other cases after
220 the first iteration (using the initial profile of $T_p(z)$) the output $\beta_p(z)$ profile showed negative values. Those cases were
associated with the proximity of the $\beta_p(z)$ and $\beta_R(z)$ values between 30 and 35 km, with the presence of noise causing
lower values of $\beta_p(z)$ than the corresponding $\beta_R(z)$, an unacceptable condition. The procedure adopted was to smooth
the measured $E_{rp}(z)$ profile in the last few kilometers and, if negative $\beta_R(z)$ values were present, reduce $E_{rp}(35)$
225 repeatedly by 0.001 until only positive $\beta_R(z)$ values exist. The second is due to the convergent iteration procedure applied
to solve the same equation (1), introducing new correction factors (a new profile of $T_p(z)$) in each step.
Taking into account those limitations we designed the re-calibration procedure. In brief it consists of several steps,
beginning with the calculation of the measured $\frac{E_{rp}(z)}{E_{rp}(35)}$ profiles inverting Equation (1) and using the same originally used
values/profiles variables. Then Equation (1) was used to calculate a first set of $\beta_p(z)$ profiles ($\beta_p^o(z)$), using all the
updated variables except $T_p(z)$. The ozone transmission, not used in the original processing (Elterman, 1966a, b), is
230 included in this step. In the next step $T_p^o(z)$ was calculated using $\beta_p^o(z)$. Finally, $\beta_p^o(z)$ is corrected by the transmission
 $T_p^o(z)$ to produce $\beta_p^{recal}(z)$, and the process stops. The iteration convergent procedure for adjusting $\beta_p^{recal}(z)$ with a new
 $T_p(z)$ was not conducted to avoid the risk of artificial enhanced $\beta_p^{recal}(z)$ because the retrieval of $\frac{E_{rp}(z)}{E_{rp}(35)}$ profiles did not
include an inverse processing of the iterative-convergent procedure Elterman (1966a, b) reported.

235 **3 The re-digitization of the searchlight 550nm aerosol extinction profiles and estimated errors**

The 105 Figures within the AFCRL report (Elterman, 1966a) consist of dots (for the total, Rayleigh + aerosol, extinction)
and crosses for the aerosol extinction, both in units of km^{-1} , plotted on a logarithmic x-axis scale, with the y-axis for
altitude, 58 points for each of the 58 elevation angles (0° to 57°) the detector was retrieving for a complete profile
observation (Elterman 1966a, b). Several of the profiles have missing aerosol extinction points above 30 km, which will
240 be discussed below.

There-digitalization process used the WebPlotDigitizer software providing among its facilities the capacity to digitize
logarithmic plotted profiles (Rohatgi, 2022). Both total extinction and aerosol extinction were re-digitized but only the
last one was used for the work reported here. The re-digitized aerosol extinction data was checked for consistency, plotted
and compared with the respective individual plots in Elterman (1966b). Then each profile was interpolated to the
245 corresponding altitude of the measurements. It was already mentioned that several of the profiles are interrupted in the
range between 30.44 km (level 52) and 34.41 km (level 57) totaling 135 missing values, representing the 21 % from 30.44
to 34.41km and 2.3 % from 2.76 to 34.41 km. In the archived datasets (Antuña Marrero et al., 2022), the missing levels
in those profiles are flagged with a missing data indicator (-999.99). Most of the missing levels were filled in with the
daily aerosol extinction profile averages, and the very few remaining were filled by linear extrapolation. Complying with
250 the assumption of an atmosphere with only two scattering components and the normalization of the detector response, the
values of the aerosol extinction profiles in the re-digitized and re-calibration profiles at the top level 58 (35.2 km) were
filled with the values of the Rayleigh (molecular) extinction at the same altitude from Table 5.9 in Elterman (1964b),
 $8.03 \times 10^{-5} \text{ km}^{-1}$.

To estimate the errors in there-digitalization process we evaluated the recovered dataset, comparing to the the tabulation
255 of data for the observations for 13 April 1964 at 00:18 MST, (Table 1 in Elterman (1966b) hereinafter named TE01. The
table shows, for each degree of the collector's elevation angle, two three variables describing the geometry of the
measurement: the scatter volume altitude (km), and scatter angle (degrees), and also the detector response (normalized),
the measured scattered signal at the detector, followed by the $\beta_R(z)$ and the $\beta_p(z)$ denoted by $\beta_R^{TE01}(z)$ and $\beta_p^{TE01}(z)$



260 respectively. $\beta_R^{TE01}(z)$ on this table matches the same variable, after interpolation, in Table 5.9 in Elterman (1964b), available at 1 km. The table covers the altitudes between 12.65 and 23.20 km corresponding to the detector elevation angles of 20° to 40°. It is important to note table TE01 is the only available source of numerical information to validate the original processing procedure.

265 We denote the original data in the Table with $\beta_p^{TE01}(z)$ and the re-digitized $\beta_p(z)$ dataset by $\beta_p^{Digit}(z)$, values at the altitudes resulting from the re-digitized station procedure and those from TE01. Figure 2 shows the vertical profiles of the logarithms of both $\beta_p^{Digit}(z)$ and $\beta_p^{TE01}(z)$ profiles for 13 April 1964 at 00:18. Their values are in the range between 10^{-2} and 10^{-4} km⁻¹, showing a very good agreement, between 12 and 23 km, the available tabulated $\beta_p^{TE01}(z)$ values, shown in figure 2.

The mean value of the differences between $\beta_p^{Digit}(z)$ and $\beta_p^{TE01}(z)$ for the entire profile section is 1.65×10^{-5} km⁻¹ an order of magnitude lower than the values in figure 1.

270 The absolute differences between the tabulated and the re-digitized Aerosol Extinction Coefficients with respect to the tabulated values is a little lower than 4% and the average is 1.2%. In the case of the altitude, using its values tabulated in TE01 and the ones re-digitized, the error produced by there-digitalization was lower than 1%.

The relative errors in there-digitalization of the altitude has a mean value of 0.08 km. The percent error of there-digitalization of the altitude, with respect to its tabulated value, shows a maximum value of 1 %, while its mean value is lower than 1%.

The results discussed above demonstrate that the errors introduced in there-digitalization procedure do not have a significant impact on the values retrieved using this procedure.

4 Retrieving the normalized detector response

280 4.1 Retrieval Procedure of the normalized detector response

The re-calibration of the searchlight aerosol extinction dataset consisted in retrieving the normalized detector response using parameters and variables that were not available in the early 1960s or have been improved afterward. In that sense the first step was inverting Eq. 1 to retrieve $\frac{E_{rp}(z)}{E_{rp}(35)}$ leading to the expression:

$$\frac{E_{rp}(z)}{E_{rp}(35)} = \left[\beta_p(z) + \beta_R(z) \frac{P_R(\varphi_s(z))}{P_p(\varphi_s(z))} \right] \frac{T_R(z)T_p(z)P_p(\varphi_s(z))}{C_1} \quad (2)$$

285 Where C_1 is a constant combining the values of several of the former variables at the normalization altitude of 35 km $C_1 = \beta_R(35) T_R(35)T_p(35)P_R(132^\circ)$.

For the retrieval of $\frac{E_{rp}(z)}{E_{rp}(35)}$ we used the original variables and parameters reported to be used for the determination of $\beta_p(z)$, all of them with the superscript “Orig” to identify them. Those variables were the re-digitized aerosol extinction profiles ($\beta_p(z)^{Digit}$), the molecular extinction profile from the Atmospheric Attenuation Model (Elterman, 1964b) for 290 550 nm ($\beta_R(z)^{Orig}$), the normalized phase functions for aerosol ($P_p(\varphi_s(z))^{Orig}$) and for molecules ($P_R(\varphi_s(z))^{Orig}$) and the molecular ($T_R(z)^{Orig}$) and the aerosol ($T_p(z)^{Orig}$) transmissions. In the case of $P_R(\varphi_s(z))^{Orig}$ it should note that it was used both for the troposphere and the stratosphere (Elterman, 1966 a,b).

4.2 Variables used for the retrieval

295 The profile of $\beta_R(z)^{Orig}$ at 550 nm is available on table 5.10 of the Atmospheric Attenuation Model (Elterman, 1964b) at 1 km vertical resolution. $P_R(\varphi_s(z))^{Orig}$ was defined by the following equation (Elterman, 1966a, b):

$$P_R(\varphi_s(z))^{Orig} = 0.75 (1 + \cos^2 \varphi_s(z)) \quad (3)$$



$T_p(z)^{Orig}$ and $T_p(z)^{Orig} \times T_r(z)^{Orig}$ were re-digitized from figure 9 in Elterman (1966a, b). $T_r(z)^{Orig}$ was calculated dividing $T_p(z)^{Orig} \times T_r(z)^{Orig}$ by $T_p(z)^{Orig}$. It is important to note that, differently to the $\beta_p(z)$ plotted profiles in Elterman (1966a) where they are represented by markers, figure 9 in Elterman (1966a) is more an artwork introducing notorious errors. However, it was the only source of information on transmission to contrast our calculus.

According to Elterman (1966 a, b) $P_p(\varphi_s(z))^{Orig}$, used to calculate $\beta_p(z)$, was derived from surface aerosol measurements conducted by the Observatory and Meteorological Institute of the University of Jena, Germany (Reeger & Siedentopf 1946), but the procedure is not explained with enough details to be reproduced. However, $P_p(\varphi_s(z))^{Orig}$ is shown on figure 4 of Elterman (1966 a,b) from which we re-digitized it. The normalization procedure applied to $P_p(\varphi_s(z))^{Orig}$ was not explicitly described by Elterman (1966a, b). However, in the common figure 4 in both cited references, the original phase function from Reeger and Seidentopf used to derive $P_p(\varphi_s(z))^{Orig}$ intercepts with $P_R(\varphi_s(z))^{Orig}$ at the normalized value 1 at a scattering angle between 40° and 60° according to the scattering angle axis labels. A later report studying atmospheric background aerosols with measurements from a balloon borne nephelometer, when it addresses the inferences from angular scattering behavior makes explicit reference to the normalization of the aerosol phase function reported in Elterman (1966b) at the scattering angle of 50° (Gibson, 1988). We determined the normalization angle solving the expression (3) for $\varphi_s(z)$ with $P_R(\varphi_s(z))^{Orig} = 1$, resulting in 55° .

$P_p(\varphi_s(z))^{Orig}$ has been considered the major source of error in determining the aerosol extinction coefficient profile from single scattering theory because it was measured at a different time and geographical location than that used for the searchlight experiment (Wells, 1968)

For the retrieval procedure all those variables were calculated or interpolated at the 58 altitudes (or their respective detector elevation angles) at which the measurements were conducted.

4.3 Retrieved normalized detector response

When deriving the normalized detector response, we use Eq. (2) and the profiles of variables identified with the superscript “Orig” and $\beta_p(z)^{Digit}$ described above, with also the variables reported in TE01, used earlier to estimate the magnitudes of any errors in the digitization procedure (see section 2.3 above). The results are shown in figure 3 where both the profile tabulated in TE01 and the one retrieved using the procedure just described are shown. They show in general a good agreement.

Errors of $\frac{E_{rp}(z)}{E_{rp}(35)}$ were calculated comparing the retrieved $\frac{E_{rp}(z)}{E_{rp}(35)}$ for 13 April 1964 at 00:18 MST with the tabulated variable profile for the same day, tabulated in TE01. Figure 3 show the retrieved $\frac{E_{rp}(z)}{E_{rp}(35)}$ profile between 2.76 and 35.28km (red asterisks) and the tabulated $\frac{E_{rp}(z)}{E_{rp}(35)}$ profile between 12.65 and 23.19 km (blue stars). Also tabulated values for the lower levels (2.76 and 3.27 km) and the top of the profile 35.28 km are shown. Except at the two lower levels, the tabulated $\frac{E_{rp}(z)}{E_{rp}(35)}$ section profile shows a good agreement with the correspondent retrieved $\frac{E_{rp}(z)}{E_{rp}(35)}$ section. It should be noted that the monotonous decrease in the retrieved $\frac{E_{rp}(z)}{E_{rp}(35)}$ is interrupted by an inflection point at 4.3 km (level 4) with the following 3 points downward decreasing in magnitude and not matching the first 2 levels tabulated on TE01. This inflection point occurs in all the 105 individuals $\frac{E_{rp}(z)}{E_{rp}(35)}$ profiles and also in the 36 daily averaged $\frac{E_{rp}(z)}{E_{rp}(35)}$ profiles as is shown in figure S1 in the Supplement. Because of this fact the re-calibration values below 5 km are recommended not to be used. Still, we will show in several cases the entire rescued and re-calibration profiles in the next sections to illustrate the impact of those



335 anomalous values. The average of the absolute differences and its percent magnitude for the 24 coincident points between
both vertical sections is 0.08 and 0.6 % respectively.

4.4 Parameters used to re-calibrate $\beta_p(z)$

4.4.1 Daily molecular extinction profiles from radiosondes

340 The benefit of using the smooth molecular density profiles derived from the Standard Atmosphere pressure and
temperature profiles to calculate the molecular extinction profile ($\beta_R(z)$) that were used in the searchlight $\beta_p(z)$ in
comparison to the less smooth density profiles derived from pressure and temperature radiosonde observations was
discussed in Elterman (1976). He cited the potential erratic, and in some cases negative, values of $\beta_p(z)$ and $T_R(z)$ when
radiosonde observations were used. However, he recognized that the use of radiosonde observations instead of the
345 Standard Atmosphere is justified in cases when the radiosondes have a good accuracy (Elterman, 1976).

That was the reason we used the Integrated Global Radiosonde Archive, Version 2 database, (IGRA-2), a global quality-
controlled set of soundings from 1905 to the present (Durre et al, 2016). It is the result of a long-term effort to produce
methods and algorithms to conduct robust automated quality control of radiosonde observed variables making available
those variables which comply with the established standards (Durre et al., 2018). We selected the nearest radio sounding
350 sites to the searchlight location with the most complete daily coverage and altitude. Witch was the Santa Teresa site, code
USM00072364 at 31.8728 °N, 106.6981 °W and 1254.0 m a.s.l. in the north of Texas. Its distance to Sacramento Peak is
130.9 km.

This dataset has a complete set of 12 UTC (05 MST) soundings for all the 36 searchlight measurements nights between
December 1st 1963 and December 31 1964. The pressure and temperature profiles of each of the soundings were
355 interpolated at 1 km vertical resolution from 1 to 30 km, linearly for the temperature and logarithmically for the pressure.
Monthly mean profiles for December 1963 and for each month of 1964 were calculated. Those mean values were used to
fill the few gaps on some of the daily profiles, all located between 22 and 30 km, mainly at the higher altitudes. Then the
pressure and temperature in each sounding, from 31 to 36 km, were filled using monthly mean values from the COSPAR
International Reference Atmosphere – COSPAR-86 (Fleming et al., 1990).

360 Filled pressure and temperature profiles for the 36 searchlight measurements nights were used to calculate the
corresponding 36 $\beta_R^*(z)$ using modern conventional algorithms (ex. Antuña-Marrero et al., 2021).

4.4.2 Molecular, tropospheric and stratospheric aerosol phase functions

The original molecular phase function $P_R(\varphi_s(z))^{orig}$ remained unchanged in the re-calibration procedure; however the
365 aerosol phase function was replaced with two phase functions, one from the surface to the lower tropopause altitude
reported from the local soundings and the NCEP-NCAR reanalysis (Kalnay et al, 1996), and the second applied above
the lower tropopause altitude to the top of the searchlight profile.

4.4.2.1 Tropospheric aerosol phase functions

370 We replaced the original aerosol phase function (APF) in the troposphere (2.76 to 10.7 km) by the tropospheric aerosol
phase function (tAPF) monthly means values calculated using almucantar sun photometer observations from the White
Sands High Energy Laser Systems Test Facility (HELSTF) AERONET site (32°38' N, 106°20' W, 1207 m asl). The site
is located in the Tularosa Basin, New Mexico, at the White Sands Missile Range. It should be considered that the Tularosa
Basin was identified above as the region where the searchlight projector was installed at least between 1963 and 1965.
375 AERONET calculates the tAPF values for 83 scattering angles at wavelengths corresponding to sky radiance
measurements (AERONET, 2022b). The monthly mean tAPF at 440 and 675 nm from 2006 to 2021 were averaged and



later interpolated between 75° and 132° at 1° resolution. Finally, the resulting tAPF at the two cited wavelengths were used to calculate the tAPF at 550 nm by interpolation.

380 4.4.2.2 Stratospheric aerosol phase functions

No phase function for the stratospheric aerosols from the 1963 Agung volcanic eruption for the northern hemisphere was found in the literature. However, we found four PSD calculated from aircraft samples taken at 18 km, from April to August 1963 in the northern hemisphere (Friend, 1966). The average of the four PSDs was calculated, and sAPF was then derived using an improved version of the Mie code (Cachorro and Salcedo, 1991). These four measurements may be heavily influenced by Agung which erupted in March 1963 and will not reflect the variations of stratospheric aerosol from 10 to 30 km, but they are the only information available for this period.

Then both the tAPF and sAPF were normalized at the angle of 55°, for the reasons explained in section 4.2. Then the normalized tAPF and sAPF were interpolated between 75° and 132° at 1° resolution. Local soundings and reanalysis (Kalnay et al., 1996) determined the lower altitude of the tropopause at White Sands during the period the measurements were conducted to be around 11 km. Then we selected 10.2 and 11.2 km in the searchlight profiles as the higher altitude of the troposphere and the lower altitude of the stratosphere respectively.

4.4.3 Molecular, aerosol and ozone transmission

4.4.3.1 Transmission algorithm

The attempts to reproduce $T_p(z)^{Orig}$ and $T_r(z)^{Orig}$, re-digitized from figure 9 in Elterman (1966a, b), using the equation (15) in Elterman (1966a, b) were unsuccessful. It could be associated with the fact that figure 9 is not exactly a plot, like the ones for $\beta_p(z)$ as we explained on section 4.2. Then, an algorithm was designed considering the geometry of the searchlight setup in figure 1. It was tested with the commercially available MODTRAN-4 atmospheric radiation transfer code, run in the transmittance mode (Berk et al., 1998) to be confident of the results of the re-calibration. In the cases of $T_R^*(z)$, and $T_{O_3}^*(z)$, the tests were conducted using the molecular and ozone profiles from the 1976 US Standard Atmosphere (U.S. Standard Atmosphere, 1976) both for the algorithm and for MODTRAN-4. In the case of $T_p^*(z)$, the aerosol extinction profile for desert aerosols embedded in the MODTRAN-4 code was used. The validation of the algorithm results showed that the mean values of the absolute percent differences between the transmission calculated using the slant path algorithm and calculated using the MODTRAN-4 code showed that transmission errors are in the order of 1% for $T_p^*(z)$ and lower than that for both $T_R^*(z)$ and $T_{O_3}^*(z)$. Details provided in figure S2 in the Supplement. For the re-calibration procedure we added the correction by ozone transmission profile ($T_{O_3}^*(z)$) that was not considered in the original aerosol extinction profiles (Elterman, 1966a, b).

4.4.3.2 Transmissions used for the re-calibration

The $T_R^*(z)$ used for the re-calibration were calculated using the $\beta_R^*(z)$ derived from the 12 UTC (05 MST) soundings for all 36 searchlight measurements nights between December 1st 1963 and December 31 1964, cited in section 4.1. Then each of the 36 $T_R^*(z)$ profiles were assigned for the re-calibration of the observations conducted the same nights. We used the ozone mean seasonal density profiles ($\mu\text{g m}^{-3}$) from the observations between 1963 and 1965 at the University of New Mexico, Albuquerque (35°N, 106.6°W) ozonesonde site (Borden and Hering, 1967). The seasonal profiles of the ozone absorption coefficient at 532 nm were calculated using the profile of ozone cross sections provided by Serdyuchenko et al., (2014) in the temperature range 193 to 293 °K, explained in detail in the Supplement of (Antuña-Marrero et al., 2021).



4.4.3.3 Other variables:

420 The monthly mean cold point tropopause altitude was also derived from the NCEP-NCAR Reanalysis (Kalnay et al., 1996) and from local soundings. The lower altitude of the monthly mean tropopause was used to determine the limit between troposphere and stratosphere to apply respectively the tropospheric and stratospheric AFPs.

4.5 Preliminary re-calibration results and subsequent adjustments

425 The first step of the re-calibration, retrieving $\frac{E_{rp}(z)}{E_{rp(35)}}$ using equation (2) and then applying equation (1) to retrieve $\beta_p^{Recal}(z)$ without transmission correction ($\beta_p^{Recal-Tr}(z)$), was conducted using the individual 105 $\beta_p(z)^{Digit}$ profiles and the updated variables corresponding to the day of the measurements: the 36 daily profiles of $\beta_R^*(z)$ and $T_R^*(z)$, the 4 seasonal $T_{O3}^*(z)$ profiles and the rest of the updated variables with no time dependence. The results showed approximately 20% of negative values and around 5% of extremely high values of $\beta_p^{Recal-Tr}(z)$ profiles which were randomly distributed in
430 time and altitude. This resembles the problem already described by Elterman (1966a; b) and solved by the normalization procedure explained on section 2.2.

Several tests showed that among the most probable reasons behind this was the hourly variability of individual retrieved $\frac{E_{rp}(z)}{E_{rp(35)}}$ profiles the same day. These were associated with the daily variability of $\beta_R^*(z)$ and $T_R^*(z)$. The natural variability of the daily $\beta_R^*(z)$ and consequently of $T_R^*(z)$, would have affected the original detector response. However, the different
435 procedures applied to the original normalized response to match the constraints imposed and the linear iterative method to adjust the aerosol extinction and the aerosol transmission, caused smoothing or spurious variability in the retrieved normalized response. That is the most plausible reason for the extreme, including negative, values generated in the retrieval described above.

Next changes were introduced in the original design of the retrieval-re-calibration procedure. The individual 105
440 $\beta_p(z)^{Digit}$ profiles were grouped daily, according to Table T1 (Supplement), and then averaged producing the daily-original aerosol extinction profiles (hereinafter $\beta_p^{Orig}(z)$). Then the first step was conducted, using in equation (2) the 36 calculated $\beta_p^{Orig}(z)$ together with the other variables $\beta_R(z)^{Orig}$, $T_R(z)^{Orig}$, $T_p(z)^{Orig}$, $P_R(\varphi_s(z))^{Orig}$ and $P_p(\varphi_s(z))^{Orig}$ described above, produced the set of 36 daily normalized detector responses (hereinafter $\frac{E_{rp}(z)}{E_{rp(35)}}^{Orig}$).

For the second step several changes were also introduced. A single profile $\overline{\beta_R^*(z)}$, the average of the 36 daily $\beta_R^*(z)$, was
445 used to calculate a single profile for $\overline{T_R^*(z)}$. The rest of the variables were unchanged. Together with the 36 daily profiles $\frac{E_{rp}(z)}{E_{rp(35)}}^{Orig}$ in equation (1) these changes produced a set of 36 daily-re-calibration aerosol extinction profiles (hereinafter $\beta_p^{Recal}(z)$).

Both in the second and third steps a change was introduced at 10.7 km, to accommodate the transition between the troposphere and the stratosphere, where sAPF and tAPF were used. This produced a discontinuity in most of the $\beta_p^{Recal}(z)$
450 profiles. A continuity solution was applied, replacing the $\beta_p^{Recal}(z)$ at 10.7 km by the average of the $\beta_p^{Recal}(z)$ values at 10.2 and 11.2 km, the levels above and below.

The retrieved $\frac{E_{rp}(z)}{E_{rp(35)}}$ profiles do not reproduce exactly the original measured $\frac{E_{rp}(z)}{E_{rp(35)}}$ ones because of the reasons described in section 2.2 and the considerations explained above. That precludes applying any new normalization-correction to the already normalized-corrected $\frac{E_{rp}(z)}{E_{rp(35)}}$ profiles. The results of the changes in the retrieval and re-calibrations procedures
455 described above produced no negative values at all for both $\beta_p^{Recal}(z)$ and $\beta_p^{Rec-Tr}(z)$.



5 Results and Discussion:

5.1 Rescued profiles of $\beta_p^{Orig}(z)$:

460 Figure 4 shows cross sections, interpolated in time and altitude, of $\beta_p^{Orig}(z)$ the daily average calculated from the individual original $\beta_p(z)$ re-digitized profiles. Higher values of $\beta_p^{Orig}(z)$ registered in the lower troposphere mainly near the lower altitude level of 2.76 km, with the maximum of $1.85 \times 10^{-2} \text{ km}^{-1}$ at 2.76 km of altitude on April 11, 1964.

Blowing dust events were defined as dust raised by the wind to moderate heights above the ground restricting horizontal visibility to less than 11 km (NWS, 1972). Reports of blowing dust from White Sands weather station (WSWS) White Sands Missile Range, New Mexico (32°23'N, 106°29'W, 1296m) from 1954-1973 and Holloman weather station Holloman (HWS) Air Force Base, New Mexico, (32°51'N, 106°05'W, 1247m) from 1960-1973 were reviewed for the period searchlight observations were conducted, December 12, 1963, to December 12, 1964. Those stations are located at 48 and 17 km respectively from Two Buttes (32°42'N, 106°08'W, 1388m) the location where the projector was installed (Hinds et al., 1975).

470 Table 1 shows the reports of blowing dust from the cited weather stations. Looking at the lower levels of the $\beta_p^{Orig}(z)$ cross sections on the days the blowing dust was reported in five of the seven reports $\beta_p^{Orig}(z)$ values are equal or higher than $7 \times 10^{-3} \text{ km}^{-1}$, the two reports in February being the exceptions. This fact contributes to the confidence on the original dataset to represent the real aerosol features in the particular conditions of White Sands.

475 5.2 Re-calibrated profiles of $\beta_p^{Recal}(z)$:

Figures 5 is similar to figure 4, except that it displays the daily average of the re-calibration cross sections $\beta_p^{Recal}(z)$. $\beta_p^{Recal}(z)$ magnitudes increase at almost all levels but particularly in the layers near the lower tropopause altitude (11 km). In the stratosphere, assuming a 10.7 km tropopause, maximum values of $\beta_p^{Orig}(z)$ and $\beta_p^{Recal}(z)$ are 6.25×10^{-3} and 1.09×10^{-2} respectively, both at 11.9 km on April 9, 1964. The increase in the maximums from $\beta_p^{Orig}(z)$ to β_p^{Recal} is 75
480 %. The existence of two aerosol layers could be identified in the cross sections for both $\beta_p^{Orig}(z)$ and $\beta_p^{Recal}(z)$, more evident in the latter, above and below 15 km.

5.3 Averaged rescued and re-calibration aerosol extinction profiles:

Figure 6 depicts the averaged profiles of $\beta_p^{Orig}(z)$ and $\beta_p^{Recal}(z)$ ($\overline{\beta_p^{Orig}(z)}$ and $\overline{\beta_p^{Recal}(z)}$), and their difference ($\Delta\beta_p =$
485 $\overline{\beta_p^{Recal}(z)} - \overline{\beta_p^{Orig}(z)}$). Almost the entire $\overline{\beta_p^{Recal}(z)}$ profile show magnitudes well above the $\overline{\beta_p^{Orig}(z)}$, except for the 3 points below 5 km, associated to the same anomalous behavior shown by the retrieved $\frac{E_{rp}(z)}{E_{rp}(35)}$ profile, shown in section 4.3. The values of $\beta_p^{Recal}(z)$ below 5 km should be considered cautiously.

Both average profiles show the two layers feature with peaks around 18 and 8 km, where average magnitudes of $\overline{\beta_p^{Recal}(z)}$ are 3.73×10^{-3} and $5.85 \times 10^{-3} \text{ km}^{-1}$ respectively. Those magnitudes represent an increase of 34 and 90 % with respect to the
490 $\overline{\beta_p^{Orig}(z)}$ magnitudes at the same levels.

The magnitudes of the AOD in the troposphere (5 to 11 km) from $\overline{\beta_p^{Orig}(z)}$ and $\overline{\beta_p^{Recal}(z)}$, are respectively 0.0181 and 0.0323, increasing 78 %. In the stratosphere (11 to 35 km) they are 0.0307 and 0.04564, corresponding to an increase of 48%.



Both the averaged $\overline{\beta_p^{Recal}(z)}$ and the corresponding AOD showed a higher increase in the troposphere than in the stratosphere.

5.4 Daily tropospheric AOD from the rescued and re-calibration aerosol extinction profiles:

In figure 7 the series of daily original tropospheric AOD (hereinafter $tAOD^{Orig}$) and daily re-calibration tropospheric AOD ($tAOD^{Recal}$) values (both from 4.8 to 10.7 km) are shown, together with the monthly mean AOD for the period 2006 to 2021 from the White Sands HELSTF AERONET site located at 1207 m asl ($AOD^{AERONET}$). This is the only nearby source of tropospheric AOD information found. It is 20 km from the projector location in Twin Buttes and 52 km from the detector at Sacramento Peak.

Both $tAOD^{Orig}$ and $tAOD^{Recal}$ agree in general with the lower values in winter of $AOD^{AERONET}$ but are in general far below during the rest of the year. The agreement in winter could be explained by contemporary estimates of the average mixing layer height diurnal cycle for White Sands were determined for the period from 1961 through 1972 using 8236 radiosonde soundings from White Sands Desert Site (32°24'N, 106°22'W and 1216 m MSL). Soundings were conducted on irregular basis with schedules depending on mission and special project requirements. The mixing height averages, and standard deviations were calculated for the entire period, every hour between 0530 to 2030 MST, for the months of December, March, June and September (Norton and Hoidale, 1976). Average mixing layer height diurnal cycle for December showed a maximum of 929 m (2,145 m MSL) at 1430 MST and minimums lower than 10 m in earliest and latest hours. In the case of June there was a maximum of 3,418 m (4,634 m MSL) at 1530 MST and minimum of 18 m at 530 MST and 137 m at 2330 MST.

During the whole year these maximum averaged values of mixing layer height are predominantly below the altitude of the lower point used for the $tAOD^{Orig}$ and $tAOD^{Recal}$ integration, 4,800 m. Then, for the entire year, only in the days when the mixing layer height is above 4.8 km the aerosols associated to the boundary layer turbulent mixing could reach above that altitude. Then only the aerosols associated to dust storms or other transport processes will contribute to the $tAOD^{Orig}$ and $tAOD^{Recal}$ shown in figure 7. However, because the observations used to calculate the $tAOD^{Orig}$ and $tAOD^{Recal}$ were conducted under meteorological favorable conditions precluding the occurrence of dust storms (Elterman, 1966a), the contribution from dust storms is not present on $tAOD^{Orig}$ and $tAOD^{Recal}$.

5.5 Stratospheric AOD from the rescued (original) and re-calibration aerosol extinction profiles:

5.5.1 Daily original and re-calibration sAOD:

Figure 8 shows the daily original stratospheric AOD (hereinafter $sAOD^{Orig}$) and daily re-calibration (hereinafter $sAOD^{Recal}$), also the monthly means sAOD for the same period after the Agung 1963 eruption in the whole northern hemisphere (Sato et al., 1993) and between 20°N and 40°N (Stothers, 2001). For the entire period from December 1963 thru December 1964 the $sAOD^{Orig}$ values are mostly lower than the monthly mean $sAOD^{Sato}$ while they match generally agree with the monthly mean $sAOD^{Stothers}$ values. The $sAOD^{Recal}$ are mainly larger than the monthly mean $sAOD^{Sato}$ and always larger larger than monthly mean $sAOD^{Stothers}$.

Table 2 shows the statistics the $sAOD^{Orig}$ and $sAOD^{Recal}$ vs. time. The mean value and maximum of the $sAOD^{Recal}$ show a 48% and 40% increase respect to the $sAOD^{Orig}$.

5.5.2 Monthly Mean sAOD:

In figure 9 monthly means $sAOD^{Orig}$ and $sAOD^{Recal}$ are plotted, together with the monthly means from $sAOD^{Sato}$ and $sAOD^{Stothers}$. In addition, in the case of the monthly mean $sAOD^{Recal}$ the 45% error estimated for the monthly mean $sAOD^{Recal}$ (see section 5.6 for details) has been plotted. The general features described in the previous subsection for both



daily sAOD series are more evident. Monthly mean sAOD^{Orig} values match in general the monthly mean sAOD^{Stothers} and at the same time are below the monthly mean sAOD^{Sato} values. In the case of the monthly mean sAOD^{Recal} values, they are always higher than ones from the monthly mean sAOD^{Stothers} and in most of the cases they are also higher than the monthly mean sAOD^{Sato} values.

540 In figure 9 could be also appreciated the decreasing trends of the monthly means sAOD^{Orig} and sAOD^{Recal}, in agreement with the well-known decay of stratospheric aerosols of volcanic origin in the years after the eruptions. However, the monthly means sAOD^{Sato} and sAOD^{Stothers} trends show an increasing tendency.

Table 3, lists the same statistical features of monthly mean sAOD as in table 2. Monthly mean sAOD^{Recal} increased 48% with respect to the mean sAOD^{Orig}, 18 % respect to mean sAOD^{Sato} and 80% respect to the mean of sAOD^{Stothers}. The monthly mean sAOD^{Recal} maximum increased 38%, 8% and 72% respect to the maximums of the monthly means sAOD^{Orig}, sAOD^{Sato} and sAOD^{Stothers} respectively.

5.6. Errors:

550 Considerations on the error of the $\beta_p(z)$ calculated profiles are discussed in detail in Elterman (1966b). It includes instrumental errors as well as the ones associated with the adjustments to the $E_{rp}(35)$ value during the iterative procedure cited above. Those adjustments consisted repeatedly reducing $E_{rp}(35)$ by 0.001 until only positive values of $\beta_p(z)$ were obtained. The maximum total errors were estimated between 33% and 48%, around 41% on average.

In the present work, in section 3, the error between the tabulated $\beta_p(z)$ and $\beta_p(z)^{Digit}$ was of the order of 2%, and the error in the re-digitized altitudes was of 0.5%. In the section 4 the error in the retrieved $\frac{E_{rp}(z)}{E_{rp}(35)}$ with respect to the tabulated 555 resulted in an error of 1%. The errors in there-digitalization and re-calibration procedure to derive $\beta_p(z)^{Recal}$ is considered as a whole 4%, increasing the error estimated by Elterman (1966b) to a range between 37% and 52%, with a 45% in average.

6. Discussion:

560 6.1 Tropospheric aerosols.

Although the goal of this work is rescuing and recalibrating the stratospheric aerosols from the Agung 1993 eruption, the aerosols in the troposphere are also of interest because of their impact on the tropospheric component of the total aerosol transmission, a very important parameter in the re-calibration process. Also their profiles could be a valuable source of information for research.

565 Contemporary studies conducted at White Sands demonstrate that searchlight measurements, conducted at night, sampled the troposphere well beyond the local boundary layer, because of the detector located at 2.76 km asl. The first of those studies reported that the low-level jet, often registered by soundings at White Sands Missile Range (WSMR), have the wind speed maximum in the upper portion (100-1000 m) of the planetary boundary layer (Rider and Armendariz, 1971). A second study reported the climatology of the mixing height (MH). In general, at night MH is minimum because of radiative cooling of the ground and heat loss from the air to the ground, reaching its maximum during the afternoon 570 because of solar heating of the ground and the subsequent heat exchange with the air. Relevant features of climatological MH at White Sands Desert Site (32°24'N, 106°22'W; 1216 m asl), computed using 8236 diurnal radio soundings from 1961 through 1972 between 5:30 and 20:30 MST (Norton and Hoidale, 1975), are shown on table 3.

Although it does not provide precise information about the nocturnal climatological MH height, the extreme hours 05:30 575 and 20:30 MST in table 4 provide a clue that the nocturnal MH was far below the altitude where the searchlight detector was located, 2.76 km, the altitude where the aerosol extinction begin.



The former conclusion implies that the boundary layer aerosol at White Sands did not reach the altitude necessary to be observed by the searchlight. That leaves only the possibility that the extinction measured in the middle-upper troposphere corresponds to dust storms or clouds. That possibility was seriously limited by the fact (described in section 2.2) that the observations were canceled in case of unfavorable meteorological conditions, including high winds and cloudy skies. This explains the relatively flat curve of tropospheric AOD derived for both the original and re-calibration aerosol extinction profiles in comparison to the monthly means tAOD bell-shaped curve from the White Sands HELSTF AERONET site between 2006 and 2021.

6.2 Digitized and re-calibration stratospheric aerosol extinction profiles

In the stratosphere the increase in the maximum values from $\beta_p^{Orig}(z)$ to β_p^{Recal} is 75 %. It is an indicator of the enhancement of the aerosol extinction after the re-calibration procedure, which is significantly higher than the estimated error in β_p^{Recal} , between 37% and 52%.

Both $\beta_p^{Orig}(z)$ to β_p^{Recal} match in general the two-layer structure and their altitudes, around 18 km for the stratospheric layer and 8 km for the tropospheric, reported from different contemporary measurements. At the same latitude the searchlight was installed Meinel and Meinel (1964) determined the mean height of the stratospheric aerosols layer to be at 17.8 km over Tucson, Arizona (32°N) late in 1963 using twilight measurements. That report corrects their preliminary estimate of 22 km (Meinel and Meinel 1963). Routine ozone soundings showed a dust layer at 20-21 km height at Boulder, Colorado (40°N) during March 1964 Pittock (1966). Measurements with a lidar at Lexington, Massachusetts (42°N), report heights of 18 km in January 1964 and 16.5 km in November 1964 (Grams and Fiocco, 1967), also present on the re-calibration profiles of this rescued dataset (Antuña-Marrero et al., 2021)

Photometric measurements on twilight photographs, the first taken by a spacecraft, from spaceship Vostok-6 over the southern coast of Africa on 17 June 1963, showed a two-layer structure, with a major aerosol layer at 19.5 km and a minor one at 11.5 km (Rosenberg and Tereshkova, 1965).

6.3 Digitized and re-calibration stratospheric aerosol optical depth

The mean of the monthly means, in table 2, show that the $sAOD^{Orig}$ is lower than $sAOD^{Sato}$, an estimate for the whole northern hemisphere, and higher than $sAOD^{Stothers}$, estimated for the 20°N to 40°N latitude band. In contrast, $sAOD^{Recal}$, is higher than both $sAOD^{Sato}$ and $sAOD^{Stothers}$ estimates. In addition, figures 8 and 9 show decreasing tendencies both for the daily and monthly means of $sAOD^{Orig}$ and $sAOD^{Recal}$ while both the trends of the monthly means of $sAOD^{Sato}$ and $sAOD^{Stothers}$ show increasing tendency. It shows the importance to try revisit the data sources used for the estimates of the sAOD from Sato et al (1993) and Stothers (2001) to evaluate the possible re-calibration of the original datasets.

One of the methods to estimate the sAOD from volcanic aerosols is the observations of changes in the Moon brightness during its total eclipses. Two observations were conducted at the State University of Iowa Observatory, 24 km west of the Iowa city (Matsushima, 1964) around 41°N, the first on 30 December 1963 (Matsushima and Zink, 1964) and the second on 19 December 1964 (Matsushima et al., 1966). A third one was conducted at the Ondřejov Observatory, 35 km southeast of Prague, Czech Republic, (49°54'55"N 14°46'52"E, 500 m asl) on June 24-25 1964 (Bouska J. and P. Mayer, 1964; Matsushima, 1967). These three astronomical observations were among a set of brightness's records from 21 lunar eclipses during 1960-1982 used to estimate the aerosols load from volcanic eruptions in that period (Keen, 1983). After converting the visual stellar magnitude to equivalent attenuations of the full moon brightness and the comparison with theoretical values of moon brightness under non-volcanic aerosols conditions, the attenuation by volcanic aerosols is calculated. Reported on table 1 from Keen (1983) the estimated $sAOD^{Eclipse}$ was 0.13, 0.08 and 0.05 respectively for 30 December 1963, 24-25 June and 19 December 1964 respectively. The $sAOD^{Eclipse}$ clearly shows a decreasing trend in



agreement with the tendency shown the daily and monthly means of $sAOD^{Orig}$ and $sAOD^{Recal}$. The nearest days in the searchlight measurements to the three cited $sAOD^{Eclipse}$ estimates and the respective $sAOD^{Recal}$ are: 30 December 1963 with 0.060, around half of the $sAOD^{Eclipse}$ 0.13; 12 June 1963 with 0.084 similar to the $sAOD^{Eclipse}$ of 0.08 and, 12 December 1964 with 0.028 which is lower than the $sAOD^{Eclipse}$ of 0.05.

The result of comparing the $sAOD^{Recal}$ with the $sAOD^{Eclipse}$ trends shows the consistency of both trends decreasing tendency. However, regarding their magnitudes, the $sAOD^{Eclipse}$ double the values of the $sAOD^{Recal}$ in December 1963 and 1964 while they have a similar value in June 1963.

7. Data availability

Data described in this work are available at PANGAEA open-access dataset repository:

Antuña Marrero, J.-C., Mann, G. W., Barnes, J., Calle, A., Dhomse, S. S., Cachorro Revilla, V. E., Deshler, T., Li, Z. and Sharma, Tropospheric and stratospheric aerosol extinction from searchlight measurements conducted at White Sands, New Mexico, US between December 1963 and December 1964., PANGAEA open-access dataset repository, <https://issues.pangaea.de/browse/PDI-32475>, 2022.

8. Summary

The rescued aerosol extinction profiles dataset and its re-calibration version that are being made available to the scientific community constitute a new piece of information that could be used for different kinds of research of the stratospheric aerosol from one of the major volcanic eruptions of the XX century. The errors in the rescuing process, conducted by digitalization of the plotted aerosol extinction profiles, has been calculated using available original tabulated data from one of the profiles, showing lower error magnitudes than the error of the retrieved aerosol extinction. The re-calibration used all the available information about the original procedure and algorithms to compute the aerosol extinction profiles and also tabulations of sections of variables used to calculate profiles. But still it was incomplete regarding the aerosol and molecular transmission, which motivated the use of the MODTRAN code run in transmittance mode to evaluate an algorithm implemented with that purpose. Another limitation was the lack of detailed information about the convergent iteration procedure applied to solve the equation (1) to adjust $\beta_p(z)$ and $T_p(z)$. That procedure introduced changes that were not possible to be accounted for in the inversion procedure from $\beta_p(z)$ to the $\frac{E_{rp}(z)}{E_{rp}(35)}$.

Because of all those limitations, comparisons of the properties of the rescued and re-calibration search light measurements with contemporary reports from several different instruments were conducted, showing reasonable agreements for both datasets. The enhancement in the re-calibration aerosol extinction profiles and in the corresponding AOD in the troposphere and stratosphere are within the ranges of the same variables from most of the other instruments.

This work is one of the very preliminary steps in the long overdue process of re-compiling, recalibrating and reconciling the existing records of the stratospheric aerosol optical and microphysical properties produced by the 1963 Agung eruption.

Supplement. The supplements related to this article is available online at:

Author contribution. LE and his team made the original searchlight measurements and its processing, reporting details and tabulated data of both activities in multiple reports and articles that allowed not only the data rescue but its re-calibration. JCAM conducted the search that found the dataset and the complementary datasets and designed and mainly conducted the re-calibration of the searchlight measurements, the error evaluation and the complementary datasets processing, with JCAM and GWM both contributing to the design of the paper and progression of the figures and text of



the article. ZL contributed with the digitization of the of the aerosol profiles, the quality control of then and preliminary data processing and analysis. JB and NS contributed with their expertise on bi-static lidar systems, also to the analysis of the searchlight results and to the selection of the tropospheric aerosol phase function. AC contributed with the calculation aerosol and molecular transmissions applying the MODTRAN code in transmission mode. VC contributed to the
665 calculation of the stratospheric aerosol phase function applying an improved Mie code she developed. TD provided advice on the specifics of the stratospheric aerosol phase function. GWM, ZL, and SD contributed to the analysis of the results. All co-authors contributed to advising/coordinating the data recovery, writing sections of the paper, and/or reviewing drafts of the paper.

670 **Competing Interests.** The authors declare that they have no conflict of interest.

Acknowledgements. To the memory of Louis Elterman and the team he led for their extraordinary achievements both technologically and scientifically. The developments of the searchlight technology they conducted had a profound impact in the early developments of lidars. In addition, their two scattering component assumption for the atmosphere, to solve
675 the searchlight equation, was also assumed to solve the lidar equation and led to its further developments. To Claudia Timmreck for contributing with the search and location of an important article to clarify the source data used by Louis Elterman for the calculation of the aerosol phase function he used in the searchlight data processing. Juan Carlos Antuña-Marrero recognizes the support from the Optics Atmospheric Group, Department of Theoretical, Atomic and Optical Physics, University of Valladolid, Spain. We also recognize role of the University of Leeds's Institute for Climate and
680 Atmospheric Science, within the School of Earth and Environment, re: the "Climate and Atmospheric Science" Masters of Research degree programme that provided ZL the opportunity to re-digitize and analyse the New Mexico searchlight measurements.

Financial Support.

685 The New Mexico 1963/64 searchlight observations recovered and re-calibrated in this study were part of a much broader program of atmospheric measurements funded by the US government within the US Air Force Cambridge Research Laboratory (AFCRL), within the meteorological section of the AFCRL program, see e.g. the two AFCRL research reports for 1963-65 (AFCRL, 1965); and 1965-67 (AFCRL, 1967), and we are grateful for the US government's support for this substantial atmospheric measurements program.

690 We acknowledge funding from the U.K. National Centre for Atmospheric Science (NCAS) for Dr. Sandip Dhomse via the UK's Natural Environment Research Council (NERC) multi-centre Long-Term Science programme on the North Atlantic climate system (ACSIS: NERC grant NE/N018001/1). The NERC standard grant project MeteorStrat (grant number NE/R011222/1) provided investigator funding for GM, and a small amount of Directly Incurred funding for ZL and SD which partly enabled this stratospheric aerosol research.

695 We also acknowledge financial support from the Copernicus Atmospheric Monitoring Service (CAMS), one of 6 services that together form Copernicus, the EU's Earth observation programme. The global aerosol development tender (CAMS43), within the 2nd phase of CAMS, provided funding for GM and SD during 2021 re: volcanic aerosol modelling, which helped enable their advice and support for the analysis of the searchlight measurements.

700 AFCRL (1965), Report on research at AFCRL for the period July 1963 to July 1965, AFCRL report 65-595, downloaded copy at https://homepages.sce.leeds.ac.uk/~amtgwm/AFCRL_ResearchReport_1963to1965.pdf
AFCRL (1967), Report on research at AFCRL for the period July 1965 to July 1967, AFCRL report 68-0039,



https://ia800703.us.archive.org/27/items/DTIC_AD0666484/DTIC_AD0666484.pdf

705

References

- AERONET, White Sands https://aeronet.gsfc.nasa.gov/cgi-bin/data_display_aod_v3?site=White_Sands&nachal=2&level=3&place_code=10 (January 5, 2022), 2022a.
- AERONET, AERONET Inversion Products (Version 3),
710 https://aeronet.gsfc.nasa.gov/new_web/Documents/Inversion_products_for_V3.pdf, Downloaded (January 5, 2022), 2022b.
- Antuña-Marrero, J.-C., Mann, G. W., Keckhut, P., Avdyushin, S., Nardi, B., and Thomason, L. W.: Shipborne lidar measurements showing the progression of the tropical reservoir of volcanic aerosol after the June 1991 Pinatubo eruption, Earth Syst. Sci. Data, 12, 2843–2851, <https://doi.org/10.5194/essd-12-2843-2020>, 2020a.
- 715 Antuña Marrero, J.-C., Mann, G. W., Barnes, J., Rodríguez-Vega, A., Shallcross, S., Dhomse, S.S., Fiocco, G. and Grams, G. W., The first ever multi-year lidar dataset of the stratospheric aerosol layer, from Lexington, MA, and Fairbanks, AK, Jan 1964 to Jul 1965, PANGAEA open-access dataset repository, <https://doi.org/10.1594/PANGAEA.922105>, 2020b
- Antuña-Marrero, J.-C., Mann, G. W., Barnes, J., Rodríguez-Vega, A., Shallcross, S., Dhomse, S. S., Fiocco, G., and Grams, G. W., Recovery of the first ever multi-year lidar dataset of the stratospheric aerosol layer, from Lexington, MA,
720 and Fairbanks, AK, January 1964 to July 1965, Earth Syst. Sci. Data, 13, 4407–4423, <https://doi.org/10.5194/essd-13-4407-2021>, 2021.
- Antuña Marrero, J.-C., Mann, G. W., Barnes, J., Calle, A., Dhomse, S. S., Cachorro Revilla, V. E., Deshler, T., Li, Z. and Sharma, Tropospheric and stratospheric aerosol extinction from searchlight measurements conducted at White Sands, New Mexico, US between December 1963 and December 1964., PANGAEA open-access dataset repository,
725 <https://www.pangaea.de/tok/2ac24d2240638ede5b2091e018f2ef1025f2d4c>, 2022
- Berk A., L. S. Bernstein, G. P. Anderson, P. K. Acharya, D. C. Robertson, J. H. Chetwynd, and S. M. Adler-Golden, MODTRAN cloud and multiple scattering upgrades with application to AVIRIS, Remote Sensing of Environment, 65, 3, pp. 367–375. [https://doi.org/10.1016/S0034-4257\(98\)00045-5](https://doi.org/10.1016/S0034-4257(98)00045-5), 1998.
- Borden, T. R., Hering, W. S., Ozonesonde observations over North America. L.G. Hanscom Field, Massachusetts: Air
730 Force Cambridge Research Laboratories, Office of Aerospace Research, U.S. Air Force, AFRCRL-64-30(IV), 365 pp., 1964.
- Bouska J. and P. Mayer, Photoelectric observation of the lunar eclipse of June 24-25, 1964. 1965, Bull. Astr. Inst. Czechoslovakia, 16, 252-254, 1964.
- Cachorro, V.E. and L.L. Salcedo, New Improvements for Mie Scattering Calculations, J. Electromagn. Waves Appl., 5:9,
735 913-926, <https://doi.org/10.1163/156939391X00950>, 1991.
- Dodd, K. N., Determination of upper atmosphere densities by scattering of searchlight beam," Great Britain, Royal Aircraft Establishment, Technical Note No. M.S. 58, Farnborough, 1959.
- Dhomse, S. S., Mann, G. W., Antuña Marrero, J. C., Shallcross, S. E., Chipperfield, M. P., Carslaw, K. S., Marshall, L., Abraham, N. L., and Johnson, C. E.: Evaluating the simulated radiative forcings, aerosol properties, and stratospheric
740 warmings from the 1963 Mt Agung, 1982 El Chichón, and 1991 Mt Pinatubo volcanic aerosol clouds, Atmos. Chem. Phys., 20, 13627–13654, <https://doi.org/10.5194/acp-20-13627-2020>, 2020.
- Durre, Imke, Xungang, Yin, Vose, Russell S., Applequist, Scott, Arnfield, Jeff. Integrated Global Radiosonde Archive (IGRA), Version 2. [Individual soundings]. NOAA National Centers for Environmental Information. DOI:10.7289/V5X63K0Q [Accessed: April,19 2022], 2016a.



- 745 Durre, I., Yin, X., Vose, R. S., Applequist, S., & Arnfield, J., Enhancing the Data Coverage in the Integrated Global Radiosonde Archive, *Journal of Atmospheric and Oceanic Technology*, 35(9), 1753-1770. Retrieved March 20, 2022, from <https://journals.ametsoc.org/view/journals/atot/35/9/jtech-d-17-0223.1.xml>, 2018.
- Elterman, L., The measurement of stratospheric density distribution with the searchlight technique, *J. Geophys. Res.*, 56, 509-520, 1951.
- 750 Elterman, L., Seasonal trends of temperature, density, and pressure to 67.6 km obtained with the searchlight probing technique. *J. Geophys. Res.*, 59, 351-358, 1954.
- Elterman, L. and A. B. Campbell, Atmospheric Aerosol Observations with Searchlight Probing. *J. Atmos. Sci.* 21, 457-458, 1964a.
- Elterman, L., Altitude variation of Rayleigh, aerosol, and ozone attenuating components in the ultraviolet region. AFCRL-64-400, 27p, 1964b.
- 755 Elterman, L., An Atlas of Aerosol Attenuation and Extinction Profiles for the Troposphere and Stratosphere. Report AFCRL-66-828, AFCRL, Bedford, Mass., 128 pp., 1966a.
- Elterman, L., Aerosol Measurements in the Troposphere and Stratosphere, *Appl. Opt.* 5, 1769-1776. <https://opg.optica.org/ao/viewmedia.cfm?uri=ao-5-11-1769&seq=0>, 1966b.
- 760 Elterman, L., Aerosol measurements since 1973 for normal and volcanic stratospheres, *Appl. Opt.* 15, 1113-1114. <https://opg.optica.org/ao/abstract.cfm?URI=ao-15-5-1113>, 1976.
- Fernald, F. G., B. J. Herman, and J. A. Reagan, Determination of Aerosol Height Distributions by Lidar, *Journal of Applied Meteorology*, 11, pp. 482-489 https://journals.ametsoc.org/downloadpdf/journals/apme/11/3/1520-0450_1972_011_0482_doahdb_2_0_co_2.xml, 1972.
- 765 Fleming, E.L., S. Chandra, J.J. Barnett and M. Corney , Zonal mean temperature, pressure, zonal wind, and geopotential height as functions of latitude, COSPAR International Reference Atmosphere: 1986, Part II: Middle Atmosphere Models, *Adv. Space Res.*, 10, 12, 11-59, doi:10.1016/0273-1177(90)90386-E , 1990.
- Friedland, S. S., J. Katzenstein and M. R. Zatzick, Pulsed searchlighting the atmosphere, *Journal of Geophysical Research*, 61(3):415-434, 1956.
- 770 Friend, J. P., Properties of the stratospheric aerosol, *Tellus*, 465, pp. 465-473, doi: 10.3402/tellusa.v18i2-3.9369, 1966.
- Grams, G. W., Optical radar studies of stratospheric aerosols, PhD thesis Massachusetts Institute for Technology, May 1966, <https://dspace.mit.edu/handle/1721.1/13502>, 1966
- Grams, G. W. and Fiocco, G., Stratospheric aerosol layer during 1964 and 1965, *J. Geophys. Res.*, 72, pp. 3,523-3,542, 1976.
- 775 Gibson, F., Atmospheric Aerosol Scattering Background Observations, AFGL- TR- 88-0146, Environmental Research Paper No.1006, 34 pp., 1988.
- Hinds, B. D., R. F. Kimberlin III, and G. B. Hoidale, "Boundary Layer Dust Occurrence. I. Atmospheric Dust over the White Sands Missile Range, New Mexico, Area," ECOM-DR-75-2, Atmospheric Sciences Laboratory, US Army Electronics Command, White Sands Missile Range, NM, 67 pp. <https://apps.dtic.mil/sti/pdfs/AD0675153.pdf>, 1975.
- 780 Hulburt, E. O., Observations of a searchlight beam to an altitude of 28 kilometers, *J. Optical Soc. Amer.*, 27, 377-382, 1937.
- Johnson, E. A., R. C. Meyer, R. E. Hopkins, and W. H. Mock, The measurement of light scattered by the upper atmosphere from a searchlight beam, *J. Optical Soc. Amer.*, 29, 512-517, 1939.
- Kalnay, E., Kanamitsu, M., Kistler, R., Collins, W., Deaven, D., Gandin, L., Iredell, M., Saha, S., White, G., Woollen, J., Zhu, Y., Chelliah, M., Ebisuzaki, W., Higgins, W., Janowiak, J., Mo, K. C., Ropelewski, C., Wang, J., Leetmaa, A., Reynolds, R., Jenne, R., & Joseph, D., The NCEP/NCAR 40-Year Reanalysis Project, *Bulletin of the American*



- Meteorological Society, 77(3), 437-472. https://journals.ametsoc.org/view/journals/bams/77/3/1520-0477_1996_077_0437_tnyrp_2_0_co_2.xml, 1996.
- Keen, R. A., Volcanic aerosols and lunar eclipses, *Science*, 222, 1011–1013, 1983.
- 790 Klett, J. D., Lidar inversion with variable backscatter/extinction ratios, *Applied Optics*, 24, pp. 1638-1643. <https://opg.optica.org/ao/viewmedia.cfm?uri=ao-24-11-1638&seq=0>, 1985
- Kovalev, V. *Elastic Lidar: Theory, Practice, and Analysis Methods*, John Wiley & Sons Inc., ISBN 0-471-20171-5, 640 pp., 2004.
- Maiman, T. Stimulated Optical Radiation in Ruby. *Nature* 187, 493–494. <https://doi.org/10.1038/187493a0>, 1960.
- 795 Matsushima, S., Site selection for a small observatory in the Midwest, *Publ. Astron. Soc. Pac.*, 76, 451, pp. 224-230, 1964.
- Matsushima, S. John R. Zink, Three-Color Photometry of Mare Crisium during the Total Eclipse of 30 December 1963, *The Astronomical Journal*, 69, 7, pp. 481-484, 1964.
- Matsushima, S., Atmospheric extinction: Czech lunar photometry of the June 25, 1964 eclipse, *Publ. Astron. Soc. Pac.*,
800 79, 178–180. DOI: 10.1086/128462, 1967.
- Matsushima, S., Zink, J. R., and Hansen J. E., Atmospheric Extinction by Dust Particles as Determined from Three-Color Photometry of the Lunar Eclipse of 19 December 1964*, *The Astronomical Journal*, 71, 2, pp. 103-110, 1966.
- Meinel, M.P., and Meinel, A. B., Late Twilight Glow of the Ash Stratum from the Eruption of Agung Volcano, *Science*, 142, 582-583, 1963.
- 805 Meinel, A. B. and Meinel, M. P., Height of the glow stratum from the eruption of Agung on Bali, *Nature*, 201, pp. 657-658, 1964.
- Niemeier, U., Timmreck, C., and Krüger, K.: Revisiting the Agung 1963 volcanic forcing – impact of one or two eruptions, *Atmos. Chem. Phys.*, 19, 10379–10390, <https://doi.org/10.5194/acp-19-10379-2019>, 2019.
- Norton C. L. and G. B. Hoidale, The Diurnal Variation of Mixing Height by Season over White Sands Missile Range,
810 New Mexico, *Mon. Wea. Rev.*, 104, pp. 1317-1320, 1976.
- NWS, Federal Meteorological Handbook No. 1, Surface Observations, Change No. 2, 1 Jan 72, 1972.
- Pittock, A. B., A thin stable layer of anomalous ozone and dust content, *J. Atmos. Sci.*, 23, pp. 538-542, 1966.
- Reeger, E. and H. Siedentopf, Die Streufunktion des atmosphärischen Dunstes nach Scheinwerfer Messungen, *Optik*, 1, pp. 15-41, 1946.
- 815 Rider L. J. and M. Armendariz, Nocturnal Maximum Winds in the Planetary Boundary White Sands Missile Range, New Mexico *J. of App. Meteorology*, 10, (6), pp.1154-1161, <https://www.jstor.org/stable/26175636>, 1971.
- Rohatgi, A., WebPlotDigitizer, <https://automeris.io/WebPlotDigitizer>, 2022
- Rosen, J. M., The Vertical Distribution of Dust to 30 Kilometers, *J. Geophys. Res.*, 69 (21), 4673-4767, 1964.
- Rosen, J. M., Simultaneous dust and ozone soundings over North and Central America, *J. Geophys. Res.*, vol. 73, no. 2,
820 479-486, 1968.
- Rozenberg, G. V., Ed., *Prozhetornyi luch v atmosfere (Searchlight Beams in the Atmosphere)*, (Izd-vo AN SSSR, Moskow, 1960), 1960.
- Rozenberg G.V., Nikolaeva-Tereshkova V.V. Stratospheric aerosol according to measurements from a spacecraft. *Izvestiya AN SSSR. Physics of the atmosphere and ocean*. V. 1. No. 4. 386-394. 1965.
- 825 Sato, M., Hansen, J. E., McCormick, M. P. and Pollack, J. B., Stratospheric aerosol optical depths, 1850 to 1990, *J. Geophys. Res.*, vol. 98, no. D12, 22,987-22,994, <https://doi.org/10.1029/93JD02553>, 1993.
- Self, S., Rampino, M.R. The 1963–1964 eruption of Agung volcano (Bali, Indonesia). *Bull Volcanol* 74, 1521–1536, <https://doi.org/10.1007/s00445-012-0615-z>, 2012.



- Schawlow A. L. and C. H. Townes, Infrared and Optical Masers Phys. Rev. 112(6), 1940-1949,
830 <https://doi.org/10.1103/PhysRev.112.1940>, 1958
- Serduchenko, A., Gorshelev, V., Weber, M., Chehade, W., and Burrows, J. P., High spectral resolution ozone absorption cross sections – Part 2: Temperature dependence, Atmos. Meas. Tech., 7, 625–636, <https://doi.org/10.5194/amt-7-625-2014>, 2014.
- Stothers, R. B., Major optical depth perturbations to the stratosphere from volcanic eruptions: Stellar extinction period,
835 1961-1978, J. Geophys. Res., vol. 106, no. D3, 2993-3003, <https://doi.org/10.1029/2000JD900652>, 2001.
- Synge, E. H., A method of investigating the higher atmosphere, Phil. Mag., 9, 1014-1020, 1930.
- Tuve, M. A., E. A. Johnson, and O. R. Wulf, A new experimental method for study of the upper atmosphere, Terr. Mag.,
40, 452-454, 1935.
- U.S. Standard Atmosphere - 1976, U.S. Government Printing Office, Washington, D.C., 1976.
- 840 Wells, M. B., Monte Carlo Analysis of Searchlight Scattering Measurements AFCRL-68-0311, AD0675153, 23 pp.
<https://apps.dtic.mil/sti/pdfs/AD0675153.pdf>, 1968.



TABLES:

Table 1: Reports of blowing dust in the vicinity of the projector location

Duration	Month	Year	Day	ToD (LST)	DD	Station
55 min.	2	1964	12	1200-1800	W	WSWS
134 min.	2	1964	14	1200-1800	SW	HWS
210 min.	3	1964	13	1200-1800	SW	HWS
403 min.	5	1964	07	1200-1800	W	WSWS
568 min.	5	1964	07	1200-1800	SW	HWS
49 min.	10	1964	02	1200-1800	C	HWS
59 min.	11	1964	03	0600-1200	NE	HWS

845

Table 2: Statistics of the Daily sAOD

Variable	Mean	σ	Max.	Min.
sAOD ^{Orig}	0.031	0.013	0.060	0.011
sAOD ^{Recal}	0.046	0.017	0.084	0.020

850

Table 3: Statistics of the Monthly means sAOD.

Variable	Mean	σ	Max.	Min.
sAOD ^{Orig}	0.029	0.007	0.038	0.018
sAOD ^{Recal}	0.043	0.009	0.056	0.028
sAOD ^{Sato}	0.040	0.002	0.043	0.036
sAOD ^{Stothers}	0.025	0.006	0.039	0.015

Table 4: Mixing height for White Sands 1961-1972

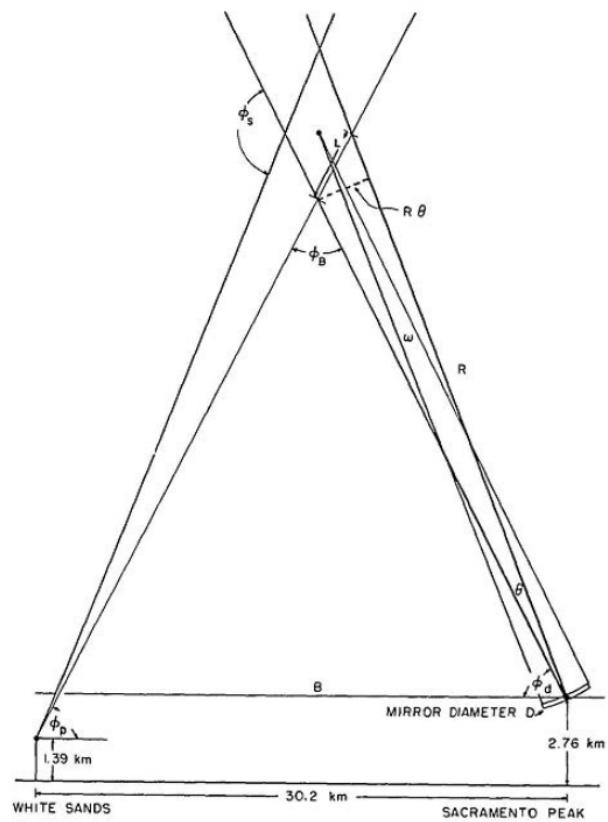
Month	Height (05:30)	Height (20:30)	Max. Height	Max. Time
December	37 m	8 m	929 m	14:30 MST
March	68 m	148 m	2,257 m	14:30 MST
June	18 m	137 m	3,418 m	15:30 MST
September	40 m	49 m	1,784 m	13:30 MST

855



FIGURES:

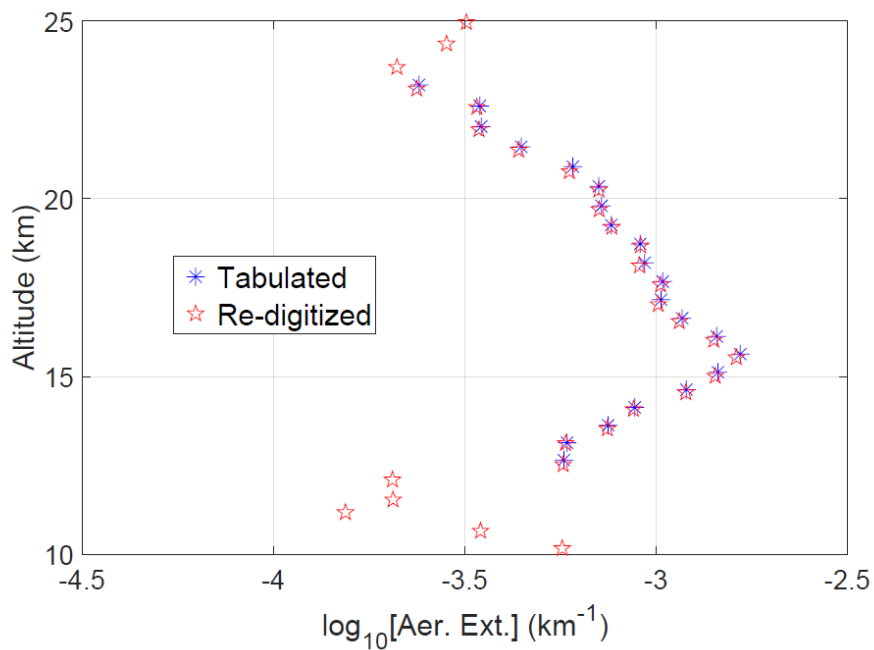
860



865 *Figure 1 Searchlight scene geometry in New Mexico. Projector elevation angle $\phi_p = 75^\circ$; beam and collector field divergences are adjusted to 1.7° and 2.0° , respectively. Both divergences are exaggerated in this figure. (From Elterman, (1966a, b)).*



870

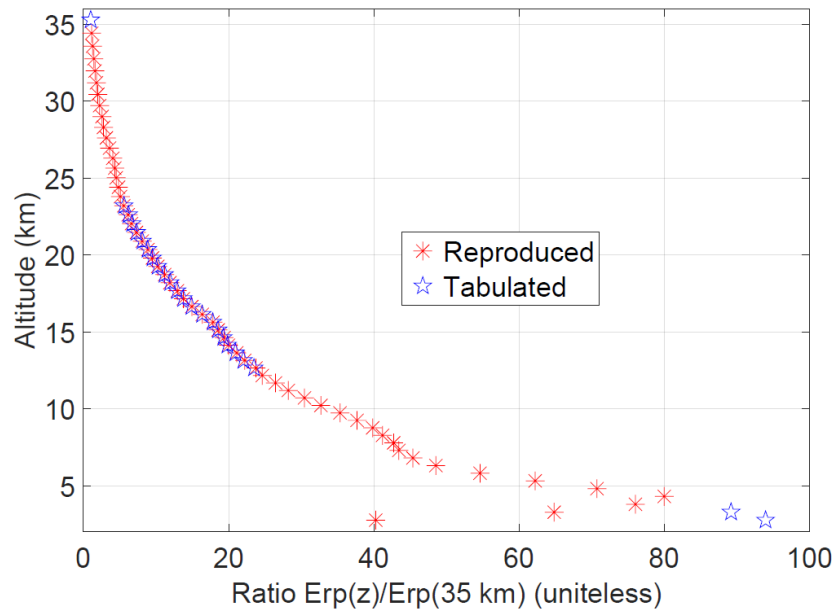


875

Figure 2: Re-digitized and tabulated aerosol extinction profile 13 April 1964 at 00:18

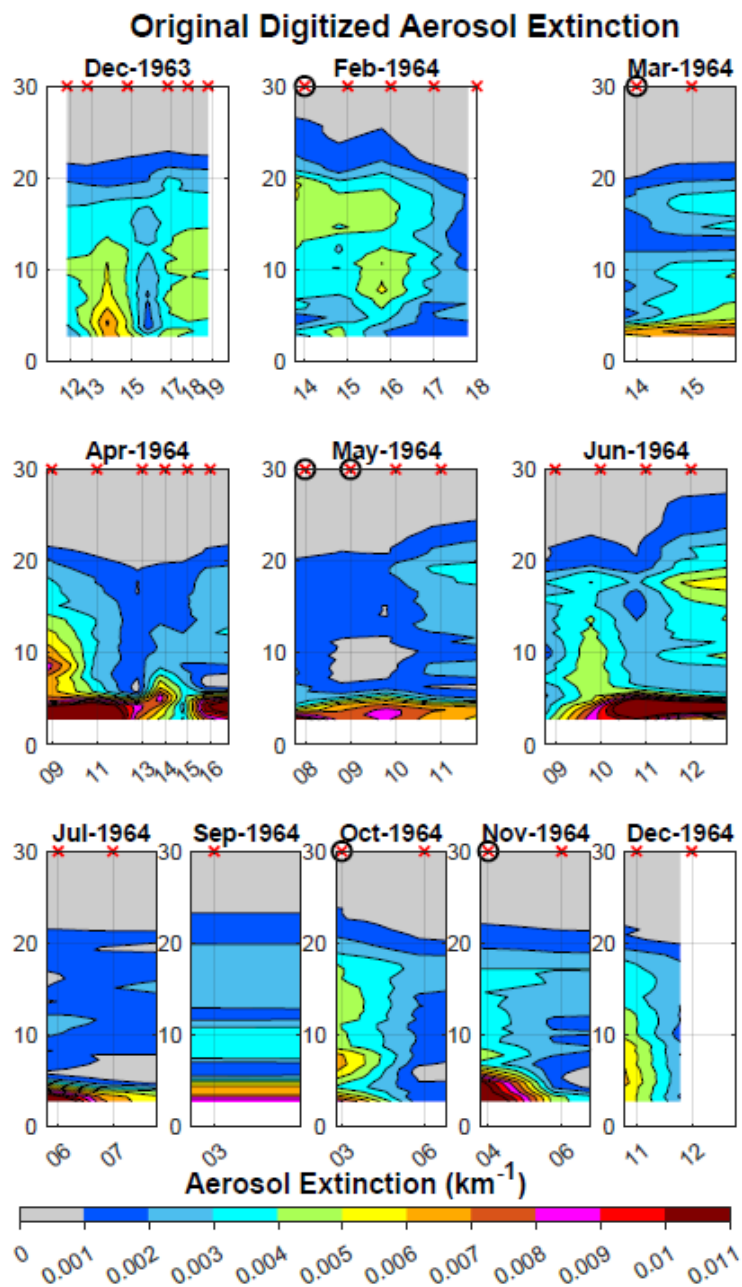


880

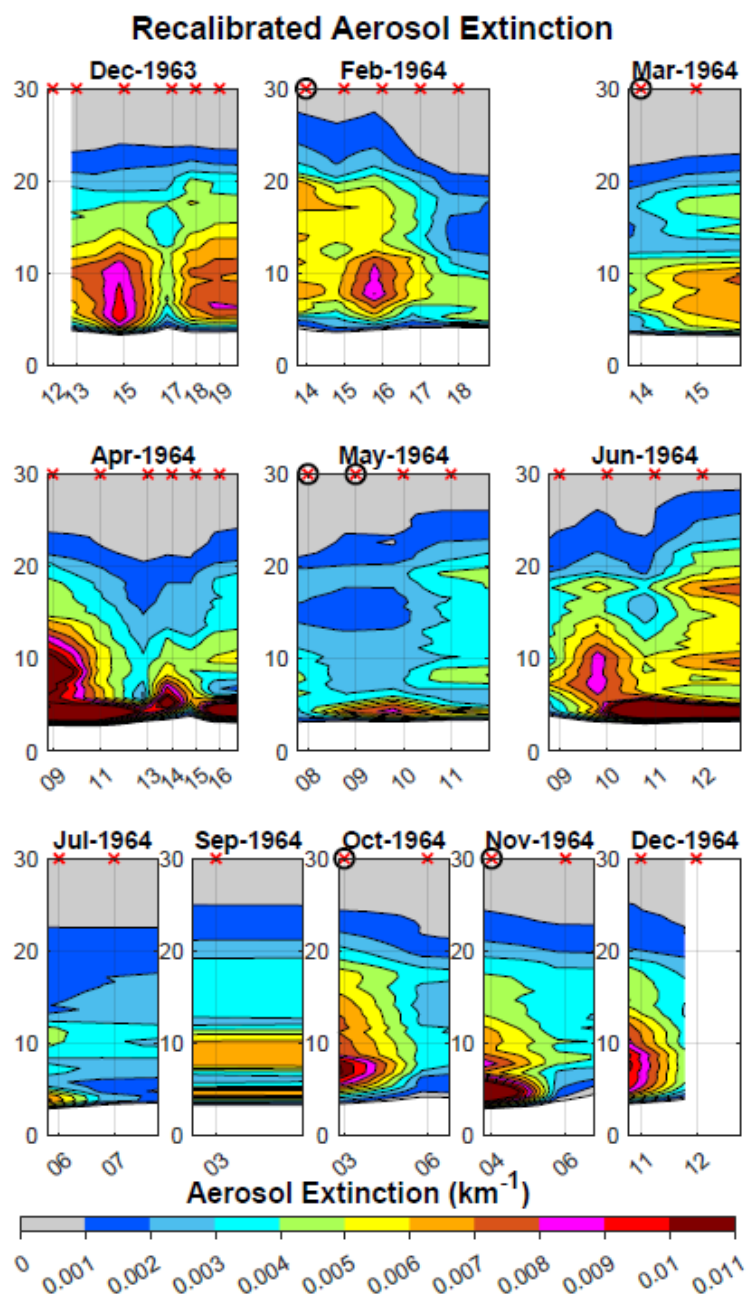


885

Figure 3: Retrieved and tabulated normalized detector response for 13 April 1964 at 00:18 MST



890 *Figure 4: Cross sections of $\beta_p^{\text{orig}}(z)$ for the set of days available each month. The red crosses on top of the panels, at the 30km altitude, indicate the dates the daily average observations were conducted. The red crosses inside a black circle indicate the day before blowing dust (visibility less than 11 km) were reported at nearby weather stations.*

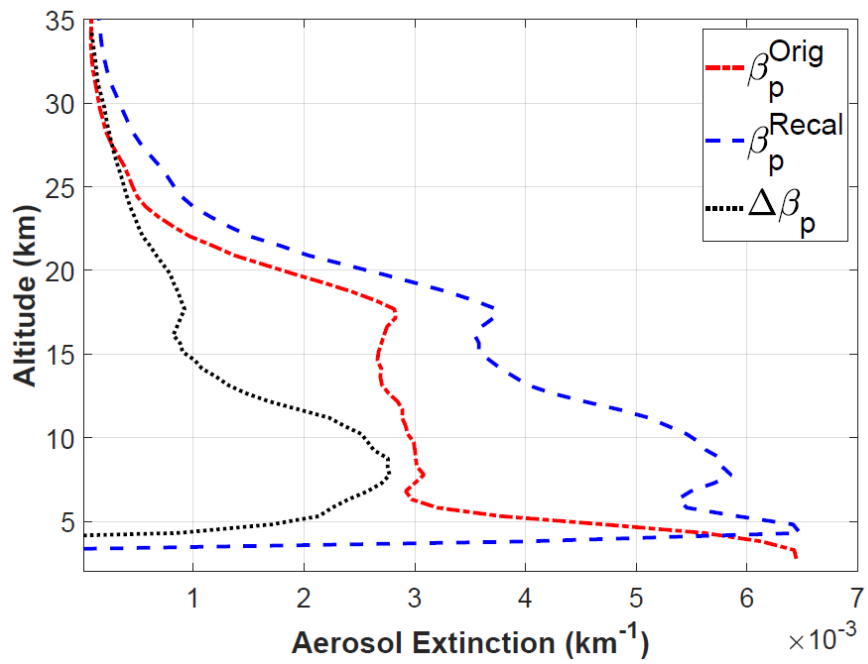


895

Figure 5: Idem to figure 5 except that it is for $\beta_p^{\text{Recal}}(z)$.



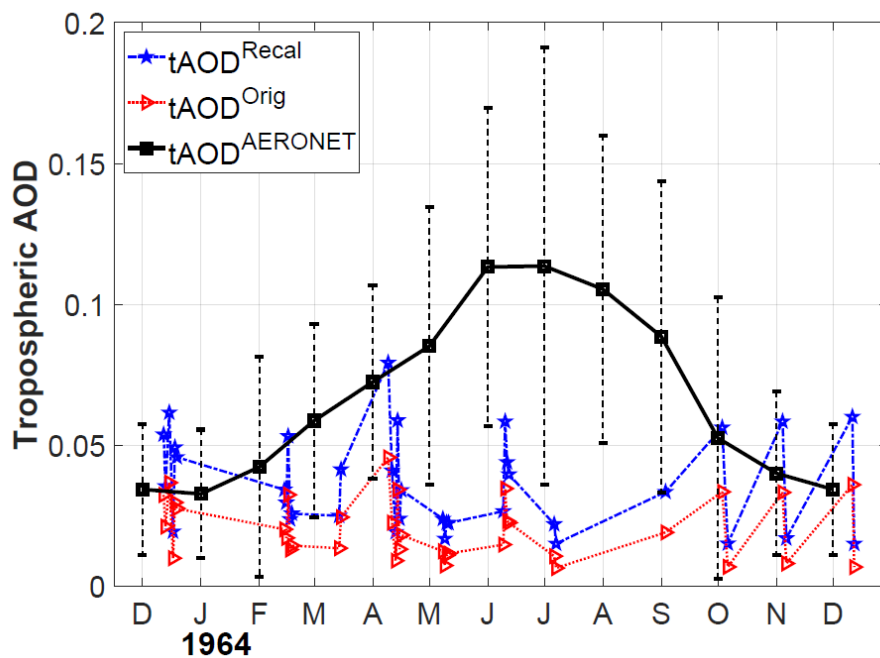
900



905 Figure 6: Profiles of $\overline{\beta_p^{\text{Orig}}(z)}$, $\overline{\beta_p^{\text{Recal}}(z)}$ and their differences $\Delta\beta_p$.



910



915 Figure 7: Time series of daily $tAOD^{Orig}$ and $tAOD^{Recal}$ (4.8 to 10.7 km). Also, monthly mean $AOD^{AERONET}$ for the period 2006 to 2021 from the White Sands HELSTF AERONET site.



920

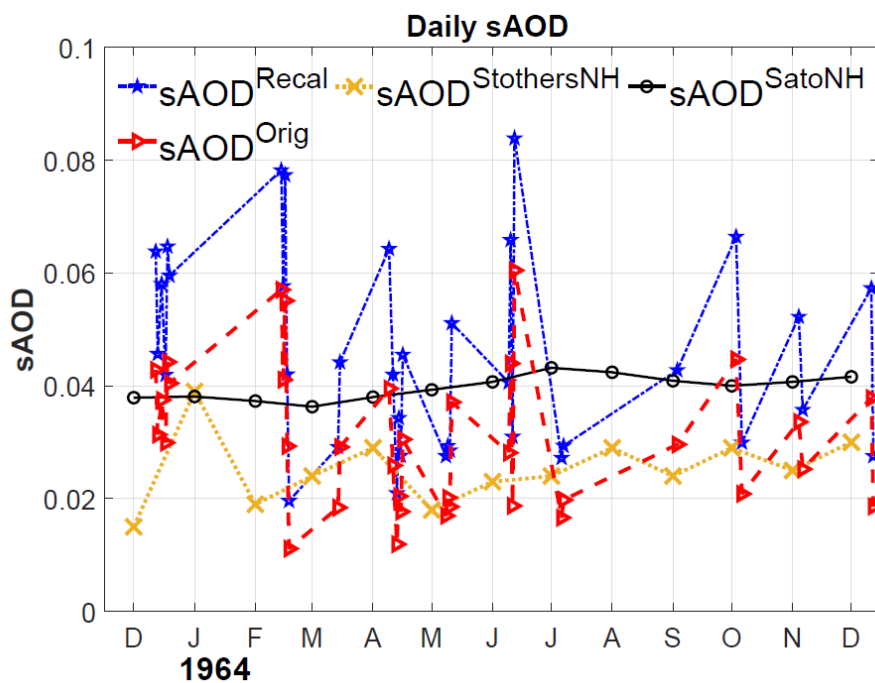


Figure 8: Daily $sAOD^{Orig}$ and $sAOD^{Recal}$ and the monthly means of $sAOD^{Sato}$ and $sAOD^{Stothers}$.

925



930

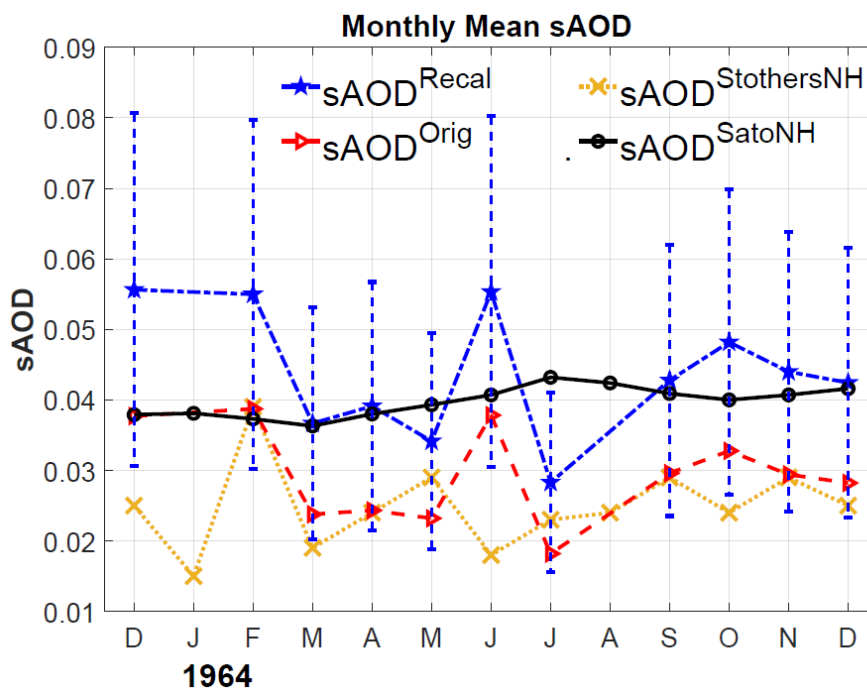


Figure 9: Monthly means $sAOD^{Orig}$ and $sAOD^{Recal}$ and the monthly means of $sAOD^{Sato}$ and $sAOD^{Stothers}$. The errors (45% of $sAOD^{Recal}$) have been also plotted.

935